Express Polymer Letters Vol.16, No.5 (2022) 500–523
Available online at www.expresspolymlett.com
https://doi.org/10.3144/expresspolymlett.2022.38

Research article

Designing a novel method for metallization polyacrylonitrile nanofiber surface by noble metallic nanoparticles: A study of synergistic relation between structural features and the mechanical/wetting properties

*Gheffar Kh. Kara, Azadeh Tadjarodi**

Research Laboratory of Inorganic Materials Synthesis, Department of Chemistry, Iran University of Science and Technology, Narmak, Tehran, Iran

Received 26 September 2021; accepted in revised form 14 January 2022

Abstract. In this research, the surface of polyacrylonitrile NFs, PAN NFs, was metalized by three noble metal nanoparticles, NM NPs, (Pt, Au, and Ag NPs, as known metalized agents) via a safe experimental protocol. Crystalline measurements showed that all traits of '$PAN_{(1\,0\,0)}$' were changed after the metallization process. An interconnection between the metallic particles and PAN possessed not only a good role in increasing the stability of the PAN chain but also in the dispersion of those over its surface, confirmed by FTIR, EDX data, and TEM images. The mechanical properties and wettability surface were tested, and results show that the nature of metalized agent clearly influences it. Owing to findings, all related values for two tests of PAN NFs increased after loading Ag NPs on its surface, but not by Pt NPs, due to the good synergistic correlation between structural features of Ag@ PAN NFs. The main focus of this paper is to study the synergistic relationship between the physical properties, according to the surficial changes of PAN NFs after metallization, and the alteration of mechanical and wetting behaviors.

Keywords:*mechanical properties, metalized polyacrylonitrile fibers, surface metallization, synergism effect, surface wetting*

1. Introduction

The polymer research institutes around the world have consecrated to prepare and design suitable polymeric structures with multiple dimensions (1-D, 2-D, and 3-D) using traditional and modern techniques to contribute to improving health society [1]. Several well-efficient techniques, such as templated assisted electro-deposition, 3-D printing templates, *etc*., have been developed to formulate a 1-D nanostructure of polymers with available structural features [1–3]. Currently, successful surveys show that electrospinning, based on applying high voltage, can be considered as a considerable (top-down) approach to generate polymeric fibrous scaffolds with unique properties. In many related scientific reports, it can be a viable method in tissue engineering for forming many categories of nanoscale electrospun fibrous webs, such as polymeric/ blends, polymeric/inorganic hybrids, and biomaterials, with unique properties [4–6]. The wide usage of the method mentioned above is attributed to its distinguished properties, among which are ease of operation, obtaining fibers with unique properties, the ability to control the diameter of the fibers, and a high surface-to-volume ratio, *etc*. [5, 6].

Recently, the metallization method has been recognized as a useful and innovative modification method for adding positive advantages to the physical and

*Corresponding author, e-mail: tajarodi@iust.ac.ir

engineering properties (modulus of elasticity, wettability, electrical conductivity, *etc*.) of different fibrous polymeric surfaces [7, 8]. Generally, most polymeric materials have poor mechanical properties, poor thermal stability, low crystallinity, low heat capacity, *etc*. [9]. Whereas metallic nanomaterials (in particular noble metals) exhibit more superior features than their polymeric counterparts, owing to good crystallinity, good corrosion resistance, very high thermal stability, high mechanical properties as well as good electrical/thermal conductivities [10]. According to an essential notion of metallization, mixing a polymer with any inorganic structure (metal, oxide, or composite) by chemical or physical methods [11], when forming a metalized polymeric fiber, is likely to fabricate a new structure with unusual properties [7, 8, 11] that each of the two components complements the properties of each other. Added metalized nano-agent can be induced the physicochemical, surface, and mechanical features of the polymeric matrix, and the polymer prevents from agglomerating the metalized agent particles through their good dispersion on the surface due to interaction between them and the functional groups of the polymeric matrix [11]. During the metallization process of polymers, the occurrence of an adequate interconnection between interacted segments of the polymeric substrate and mineralized reactants in all metallization stages can attain by four mechanisms, namely mechanical or interlocking, weak boundary, chemical and electrostatic mechanism, which have been reviewed by Mittal [11]. According to many kinds of literature [7, 8, 11], it can be concluded that the conditions applied to mineralize the surfaces of polymeric substrates were uneconomical and unsafe because having many problems such as releasing of toxic gases, the multiplicity of initial stages of the polymer surface preparation, complex equipment and actuators to operate and others [7, 11, 12]. For example, the use of physical vapor deposition (PVD) method requires metal sublimation at high temperatures and also needs a covering substrate with a layer or etching to deposit the metal layer on it [12]. Therefore, this method has been beneficial to some resources. Up to now, the publications' number in the field of the synthesizing of metalized fibers in the presence of a wide spectrum of metallic nanoparticles has been enhancing dramatically [13]. These products have received rapid attention in several futuristic applications such as energy storage and electronic devices [14], remediation of contaminants [15], lithium battery [16], restoration of damaged tissues [17], and so on.

One of the most important and popular polymeric substrates in preparing this type of formulation is polyacrylonitrile (PAN). Its fibers occupy the third rank among all synthetic fibers in production [18, 19]. The great interest in polyacrylonitrile fibers is due to its many virtues such as high mechanical strength, thermal and chemical resistance, as well as low price, carbon content (up to 56%), possibility of obtaining fibers possessing various thicknesses and diameters, heat treatability, high resistance to ultraviolet irradiations/acids and weak bases [18, 19]. Several studies confirmed the increase in the stability of polyacrylic nitrile fibers after preparing them by the electrospinning method, through applying oxidation under heating conditions at high temperatures [19, 20]. Amongst them, Katepalli's research aimed to increase the stability of PAN NFs by applying sequential oxidation conditions at temperatures up to 250 °C [20]. The obtained results showed the formation of effective functional groups (C=O, O–H, C=N, C≡N, *etc*.), transforming the linear structure to a ladder structure with strong crosslinking and high carbon content in the final fibers [20]. Nataraj emphasized in his review that the preparation of carbon nanofibers of PAN includes four stages (electrospinning, oxidative stabilization, and carbonization). The last two stages require high temperatures under aerobic conditions that allow the induction of the cyclization reaction of the nitrile groups, reduction of C≡N groups to C=N groups, and the creation of potent intramolecular bonds with forming of toxic violate compounds (cyanide gas, carbon monoxide, ammonia, and others) [19]. The great challenge in this regard is the displacement of the imitative modification stages and utilized modifiers (for example, carbon compounds, silicate, or metallic nanoparticles) by applying more available conditions (lowering the treatment temperature) to get the desirable metalized fibers of PAN [19]. The restoration of basic deficiencies (crystallization degree, crystal size, and orientation) and, in return, the surface properties of those NFs are directly affected by the change of the size of mineral additives, the size of fibrous diameters, porosity, particle shapes, etc. [21]. Shilpa and Sharma [22] offered a study on the electrospun hollow NFs loaded with dispersed Ag NPs at high temperature and their electrochemical

behaviors as the anode in energy cells. The paper by Karimi-Maleh *et al*. [23] has cited that the metallization process was performed by pyrolyzation Palladium–Nickel nanoparticles/functionalized-MWCNT and employed as a sensitive non-enzymatic electrochemical glucose sensor. The novelty of this paper focused on three essential aspects, as follows: (i) the safety of the protocol used for metallization surface of PAN NFs by incorporating two consecutive environmentally friendly ways (electrospinning 'ES' + ultrasound irradiation 'USI'). In contrast to the rest metallization protocols in harsh conditions, the method used was not accompanied by the formation of any toxic substance or the release of toxic gases during preparation. Therefore, the method used can be described as the green method. (ii) In this paper, we presented a detailed synergistic study by defining the correlation between the crystallinity degree and the rest of the other structural features for all synthesized fibers, compared to other researches that were limited to the characterization of the fibrous structure after metallization with one type of metal. (iii) The mechanical properties and wettability of all metalized fibrous surfaces were evaluated. Furthermore, a close relationship was found between mechanical properties and wettability of all metalized fibrous surfaces and their structural synergism.

2. Experimental section

2.1. Chemicals

The materials used in this study were hydrogen tertrachloroaurate (III) trihydrate ($HAuCl_4 \cdot 3H_2O$ with purity 99.99%), hydrogen hexachloroplatinate (IV) hexahydrate ($H_2PtCl_6 \cdot 6H_2O$ with purity ≥37.50% Pt basis), and silver nitrate ($AgNO_3$, crystal extra pure, which were supplied by Merck company (China). Polyacrylonitrile ($(C_3H_3N)_n$, 150 000 M_W, co-polymerized with 1 wt% methyl acrylate), *N*,*N*-dimethyl formamide (DMF), hydrazine hydrate ($N_2H_4 \cdot H_2O$), ammonia solution (25% solution) were acquired from Sigma-Aldrich. All the reagents were used as received without further purification in this study.

2.2. Preparation of NM NPs

NM NPs were prepared by the reaction of ion metals and reduction system (DMF/$N_2H_4 \cdot H_2O$) in the presence of ammonia solution (25%), by a USI as follows:

H_2PtCl_6, $HAuCl_4$, and $AgNO_3$ solution as Pt, Au, and Ag sources were used, respectively. Briefly, at first, 7 ml (0.05 M of H_2PtCl_6 solution), 7 ml (0.05 M of $HAuCl_4$) and 7 ml (0.05 M of $AgNO_3$) were separately mixed with 10 ml DMF. Next, the mixture was kept at 75 °C in an oven for 90 min. After that, the solution was irradiated in a bath ultrasound for 20 min at 75 °C under an aerobic atmosphere. At the same time, 220 µl of freshly prepared (0.0015 M) hydrazine hydrate solution was dropped slowly into the solution. The pH of the solution was adjusted to 10 with ammonia solution to allow for a complete reduction reaction. The reactants were continuously sonicated at 75 °C and at power 40 W/m^2 for 20 min. In the subsequent stage, the samples were centrifuged at 7000 rpm and washed with a mixture of EtOH/H_2O (20:3 v/v) and then dried under vacuum at 95 °C for 10 h. The schematic illustration of the NM NPs preparation is shown in Figure 1 (Step 1).

2.3. Preparation of as-spun polymeric solution

In a typical preparation of the precursor polymeric solution, 0.81 g PAN powder was firstly dissolved in 9.5 ml of DMF. Then, the PAN/DMF solution was stirred for 3 h at room temperature with vigorous stirring. This solution was heated at 75 °C for 18 h under aerobic in order to obtain a yellowish-color homogeneous solution, as shown in Figure 1. This stage of preparation mainly aimed to modify the surface of the polymeric matrix by changing the polymer structure (from linear formula to cyclic formula) with abundant contents of active functional groups, which can be able to interact with the particles. By mentioned to reference [24–31], the color change of the polymeric solution (from transparent (Image A in Figure 1 (Step 2)) to yellowish-color (Image B in Figure 1 (Step 2)) is clear evidence of the structural change in the polymeric matrix.

2.4. Preparation of electrospun NM@ PAN NFs

In this step, 0.27 g of NM NPs was separately re-dispersed in 3.5 ml DMF solution for 30 min by using bath ultrasound at power 40 W/m^2. Next, this solution was slowly dropped to the above PAN/DMF solution, that the mass fraction of PAN in the DMF solution was 6 wt%, and was heated at 75 °C under the continuous magnetic stirring for 2 h. The electrospun M@ PAN NFs from the related solution containing NM NPs at 10 wt% on a total solute basis were donated as Pt@ PAN NFs, Au@ PAN NFs, and Ag@ PAN NFs, respectively. An electrospun solution was

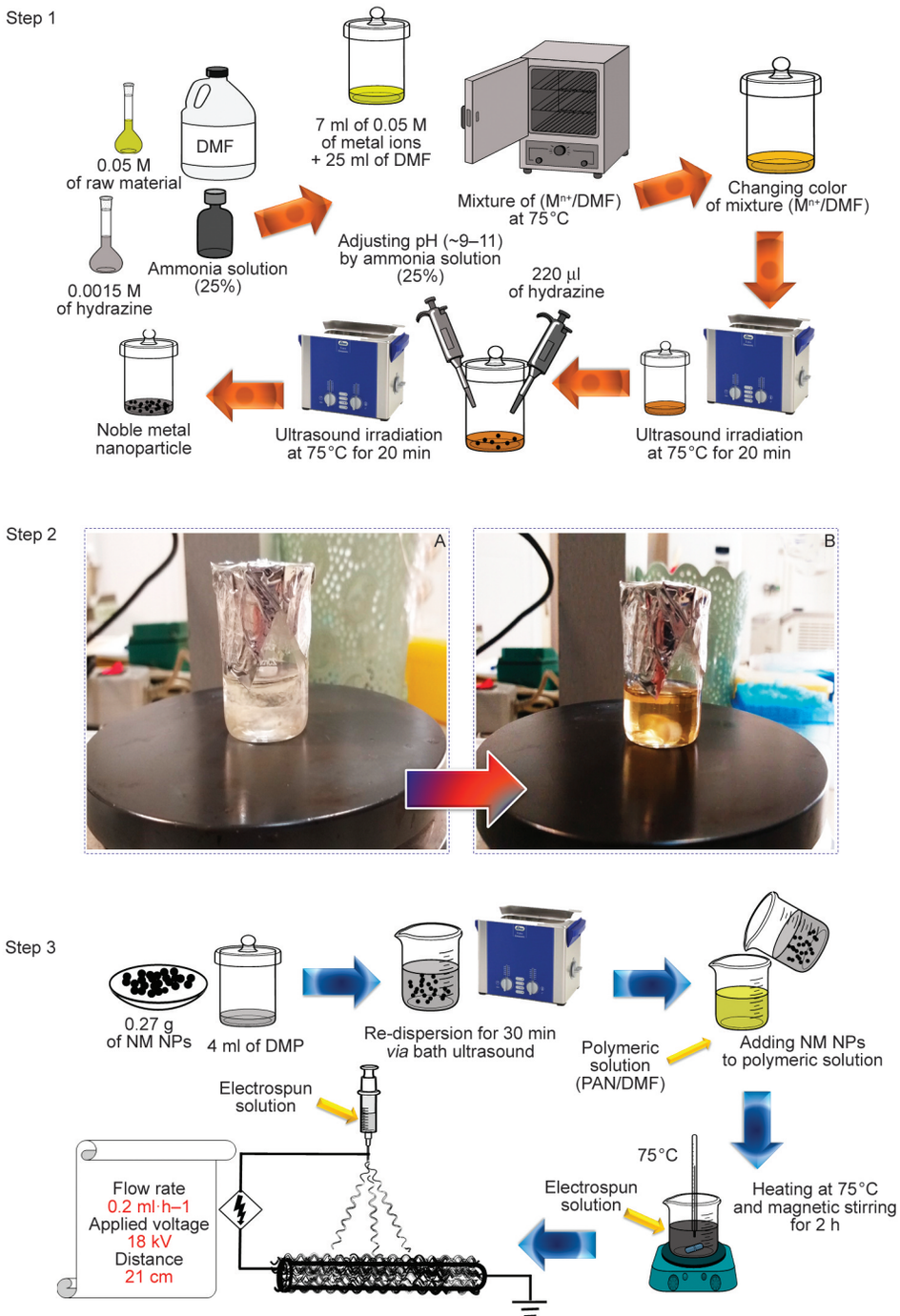

Figure 1. *Ex-situ* synthesis chart for the preparation of NM NPs in the reduction system (DMF/$N_2H_4 \cdot H_2O$) and ultrasound irradiation (Step 1), surface modification of PAN in non-harsh condition (T = 75 °C, t = 18 h, O_2) (A) digital image of transparent solution of PAN/DMF after stirring for 3 h at 25 °C and (B) digital image of yellowish-color solution of PAN/DMF after stirring for 18 h at 75 °C) (Step 2) and schematic illustration for the preparation of M@ PAN NFs via ES (Step 3).

transferred into a syringe with a capacity of 10 ml and an inner diameter of about 0.8 mm. The positive voltage connected with the tip of the syringe was approximately 18 kV, the distance from the tip to the rotating drum was 21 cm, and the rotary speed of the drum was 300 rpm. The feeding rate of the precursor solution was 0.2 ml/h. Step 3 in Figure 1 shows the fabrication of metalized PAN NFs based on the loading of NM NPs on their surface.

2.5. Apparatus

X-ray diffraction (XRD) patterns were recorded on an X-ray diffractometer (X' pert pro. Analytical company) using Cu-Kα radiation (λ = 1.5406 Å, the

scanning rate of 0.02 2θ/sec, at 40 kV and 40 mA). The morphologies of M@ PAN NFs were characterized by field-emission scanning electron microscopy (FESEM) (FESEM-ZISS-Sigma VP-Germany) with an acceleration voltage of 3 kV and transmission electron microscopy (TEM) (TEM-ZEISS- EMIOC, operating at 100 kV). A FESEM equipped with an energy-dispersive X-ray analyzer and elemental mapping (Oxford Instrument company-England) were used to determine the morphology and composition of the as-prepared samples. The diameter of fibers and the size of metalized agents were computed from the FESEM images by Image J software. At least seventy NFs were utilized to obtain the required diameters and sizes for each sample. Topographical images of the various fibers were obtained using atomic force microscopy (AFM) (JPK NanoWizard® AFM system) with no pre-imaging preparation. Fourier-transform infrared (FT-IR) spectra were recorded on a Shimadzu FT-IR-8400 spectrophotometer using a KBr pellet for sample preparation.

2.6. Measurements

Debye-Scherer's formula was used to calculate the average crystalline size of the nanoparticles from the broadening of a peak in a diffraction pattern, according to Equation (1) [32]:

$$D = \frac{0.96\lambda}{\beta \cos\theta} \tag{1}$$

where 'β' is full at width half maximum (FWHM), 'λ' is the wavelength of Cu Kα (1.5406 Å) of radiations, 'θ' is the Bragg's angle and '*D*' is the mean crystallite size of the sample. Also, the crystallinity degree (*Z*) of all electrospun samples is determined from their XRD data by using Equation (2) [32]:

$$Z = \frac{I_d}{I_t} 100 \tag{2}$$

In equation (1), the '*Z*' is the average of the crystallinity, 'I_d' is the intensity of their diffraction peaks, and 'I_t' is the sum of the intensities of these samples. To show the strength of the active link between the M NPs and the functional nitrogen groups in the conjugated aromatic rings and the contribution of these mineral combinations to the stability of the proposed final structure of the polymer during the final stage of the experimental section (1.4. stage), the degree of relative cyclization rate (*RCR*), as demonstrated in Equation (3), for each fabricated fiber is calculated using the data of the paper's Qiao *et al*. [33]:

$$RCR = \frac{I_{C=N}}{I_{C=N} + I_{C\equiv N}} 100 \tag{3}$$

As described in Equation (3), $I_{C=N}$ is the transmission of the double stretching bond of C=N, while $I_{C\equiv N}$ is the transmission of the triple stretching bond of C≡N.

2.7. Evaluation of engineering properties

Tensile measurements were applied on a standardized testing machine (STM-20, SANTAM, Tehran, Iran) to understand the mechanical behavior and associated properties of each one of the synthesized fibrous samples (before and after the metallization process). The fibrous specimens constructed for these measurements were machined using traditional methods of mechanical testing. For this, samples were cut into rectangular shapes with dimensions (length 4 cm × breadth 1 cm). These measurements were executed under ambient conditions using a load cell of 10 N and a crosshead velocity of 5 mm/min. Three replications were measured for each sample at the same conditions. The obtained results were plotted in (stress-strain) curves, and all mechanical parameters (ultimate tensile strength 'σ', Young's modulus '$\ddot{Y}$' and elongation at break '$\ddot{E}$') were elicited from it. It is stated that the former variables were reported as means ± standard deviation (SD).

2.8. Wetting surface study

To check the influence of the metallization of the PAN NFs surfaces on hydrophilicity property, the *WCA* was evaluated for the whole fibrous surfaces. The *WCA* measurements were done in the following: 5 µl of distilled water on the sheet of each sample was horizontally deposited *via* micropipette. These measurements were repeated from at least three consecutive times in different sites on the surface of the sample, and the final water droplets were simultaneously viewed using a high-resolution camera from parallel direction to the fibrous orientation and its related profile is analyzed by using a suitable made program (Digimizer program).

3. Results and discussion (physiochemical characterization)

The synthesized M@PAN NFs by ES route were examined by different characterization techniques

(XRD, FESEM, TEM, EDS-SEM mapping images, AFM and FT-IR).

3.1. XRD patterns

The X-ray diffraction patterns of metalized agent powders, PAN NFs, and their metalized NFs at various loadings of metalized agents were introduced in Figure 2. The reports of the corresponded XRD data for both components (metalized PAN NFs and metalized agents) and the calculated lattice parameters (*d*, *D*, and *Z*% of the hexagonal system 'PAN$_{(1\,0\,0)}$') were listed in Tables 1, 2. The represented XRD pattern of the PAN NFs, as given in Figure 2a, shows that this specimen has two distinct peaks with a difference in the crystalline characters. The first intense is a sharp peak (1 0 0) plane located at 2θ = 17.28° for the hexagonal lattice of those, while the other is a weak peak (0 2 0) plane at 2θ = 27.06°. These two peaks with different intensities at 2θ = 17.28 and 27.06° can be attributed to the dual crystalline structure of PAN NFs, exhibiting a strong intermolecular interaction among these cyanide groups or reflecting the distance conversion in the molecular chains and/or molecular segments [32, 33]. According to Qiao's study [33], the functional groups of C≡N tended to reduce to C=N groups, which also tended to conjugate together to form the untidied cyclized structure of PAN molecules. Thus, we believed that the reduction process of C≡N groups was more increasable under thermal oxidation for a long time. These formed groups of the cyclized structure are taken place in multi places between the arranged separators of the molecular chains in the PAN, and as a result, a disturbance occurred in the arranged molecular system of PAN. These findings meant that the PAN NFs contained two crystalline phases (well-crystallized phase and a few amorphous phases). Figure 2c shows the X-ray diffraction pattern of all as-prepared metalized PAN NFs. The crystalline metalized fibers showed that each metalized agent possessed five distinct diffraction peaks and the labeled crystallography planes by Miller indices (*h k l*) for each one. The Pt@ PAN NFs, Au@ PAN NFs, and Ag@ PAN NFs showed the diffraction peaks Pt (1 1 1) located at 2θ

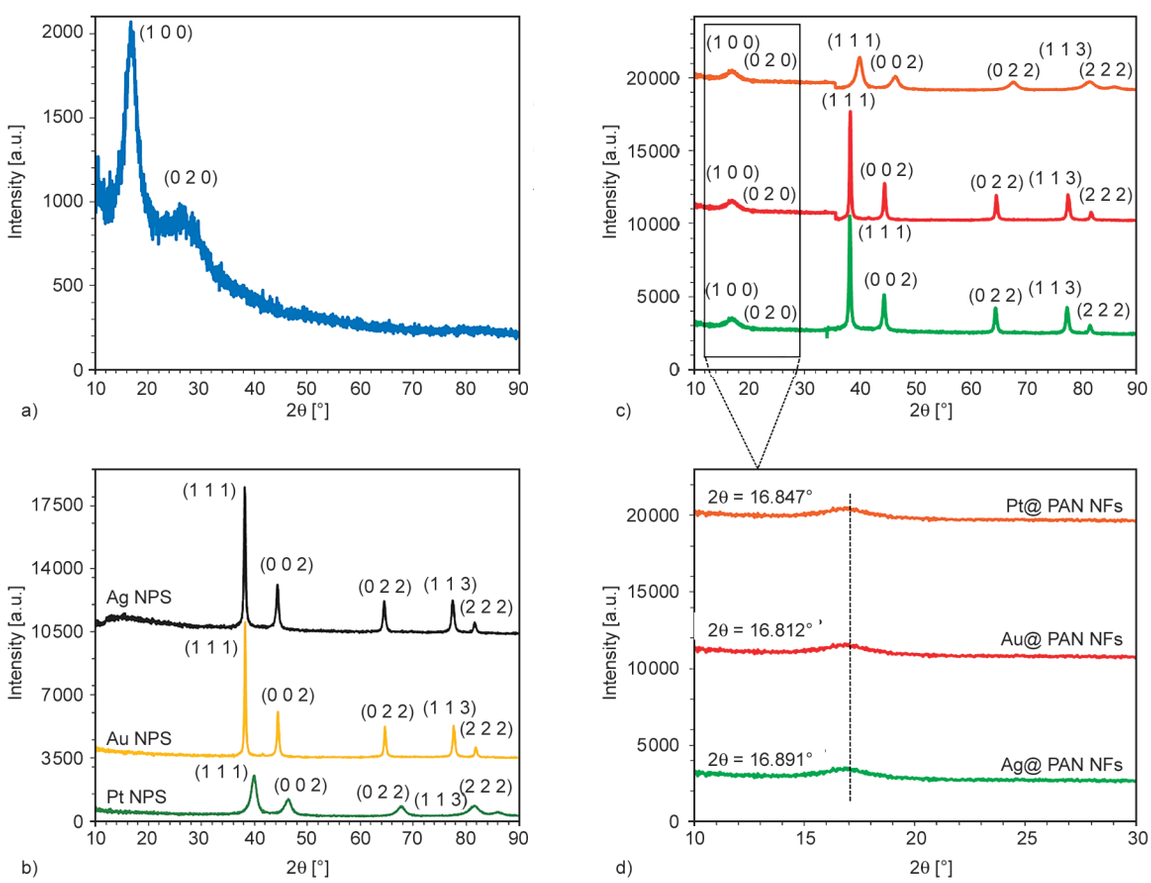

Figure 2. XRD patterns of all electrospun NFs, (a) PAN NFs, (b) metalized agent powders, (c) Au@ PAN NFs and Ag@ PAN NFs in the range of angle diffraction (10–90°), (d) the part of M@ PAN NFs in the range of angle diffraction (10–30°).

values of 39.89°, Au (1 1 1) centered at 2θ values of 38.19° and the obvious diffraction peak Ag (1 1 1) located at 2θ = 38.11°, respectively. These results indicated that all metalized agents were related to the face-centered-cubic (FCC) structure, and the crystalline data for each one was given in Table 1. The growth orientation of M (0) common in a fixed direction (1 1 1) belonged to strong diffraction at unique diffraction angle peak for each one. The growth of Au and Ag particles returns to the formation of molecular-sized solids: (i) formation by replicating three-dimensional patterns of each atom, (ii) enlarging those solids with the uniform distance between each component [34]. As for FCC Pt metal, the low-index surface of {1 1 1} facets, difference surface energy of the crystalline plane in the presence of many morphologies [35], and the interplane variation distances of {1 1 1} via the large size of particles were considerably reasons for explanation Pt growth in direction (1 1 1), which were preferentially reviewed by Boita *et al*. [36]. The whole diffractometer profiles of metalized fibers and powders, as depicted in Figure 2b, clearly suggest that each of NM NPs loaded on the PAN NFs was composed of metal crystals only, and no other compounds such as oxides exist. Therefore, the reduction reaction of metal ions (M^{n+}) to zero-valent silver (M (0)) was complete. As shown in patterns of Figure 2c, it can be noted that the changes on the main position peak at 17.28° of PAN are based on the type of the metal and different sizes of crystals. Additionally, from Table 1, it can be induced that there was a difference in the (*Z*%, *D*, and *d*) values of the major (1 0 0) diffraction because of effective interaction between NM NPs and PAN.

Table 1. Description of XRD information of all electrospun samples.

Sample	XRD crystal plane	*d* [nm]	*D* [nm]	*Z* [%]
PAN NFs	(1 0 0) (1 1 0)	0.5260 0.3231	3.42	60.55
Pt@ PAN NFs	(1 0 0) (1 10)	0.5636 0.3741	41.67	27.57
Au@ PAN NFs	(1 0 0) (1 1 0)	0.5696 0.3321	34.53	32.15
Ag@ PAN NFs	(1 0 0) (1 1 0)	0.5582 0.3381	40.14	40.14

Table 2. Summary of lattice parameters of PAN NFs and loaded metalized agent in all electrospun samples (M@ PAN NFs).

Sample	Lattice parameters
PAN NFs[a]	JCPDS file (96-432-8472), $a = b = c = 32.49$ Å Space group: $R\bar{3}$ Crystal system: Hexagonal Calculated density: 1.16 g·cm^{-3} Volume of cell (·10^{-6}) = 14932.19 pm^{-3}
Pt@ PAN NFs[b]	JCPDS file (96-901-2958), $a = b = c =$ 3.91 Å Space group: Fm$\bar{3}$m Crystal system: FCC Calculated density: 21.66 g·cm^{-3} Volume of cell (·10^{-6}) = 59.82 pm^{-3}
Au@ PAN NFs[c]	JCPDS file (96-900-8464), $a = b = c = 4.07$ Å Space group: Fm$\bar{3}$mCrystal system: FCC Calculated density: 19.47 g·cm^{-3} Volume of cell (·10^{-6}) = 67.17 pm^{-3}
Ag@ PAN NFs[d]	JCPDS file (96-110-0137), $a = b = c = 4.09$ Space group: Fm$\bar{3}$mCrystal system: FCC Calculated density: 10.50 g·cm^{-3} Volume of cell (·10^{-6}) = 68.22 pm^{-3}

[a]Crystal lattice parameters data related to polymer alone.
[b]Crystal lattice parameters data related to loaded Pt NPs alone (Pt card (JCPDS-96-901-2958, and the crystallographic parameters (space group: Fm$\bar{3}$m, lattice parameters: $a = b = c = 3.91$ Å).
[c]Crystal lattice parameters data related to loaded Au NPs alone (Au card (JCPDS-96-900-8464, and the crystallographic parameters (space group: Fm$\bar{3}$m, lattice parameters: $a = b = c = 4.07$ Å).
[d]Crystal lattice parameters data related to loaded Ag NPs alone (Ag card (JCPDS file number (96-110-0137) and the crystallographic parameters (space group:Fm$\bar{3}$m, lattice parameters: $a = b = c =$ 4.08 Å).

3.2. FESEM and TEM micrographs

FESEM and TEM micrographs of the surface morphologies of the electrospun bare polyacrylonitrile and their metalized NFs at different magnifications have been given in Figures 3 and Figures 4, respectively. In Table 3, separate detailed explanations of each metalized fiber were provided with the appropriate FESEM pictures. FESEM micrographs for the bare PAN NFs (Figures 3a–3c) elucidate that these fibers consist of a downy surface with a moderate diameter distribution of 268±3 nm. The as-spun PAN NFs do not possess beads. The high-resolution FESEM graphs of Pt@ PAN NFs have been displayed in Figures 3d–3f, where a relative tubercular surface with an average of them about 391±4 nm was clearly marked. The surface of PAN NFs was surrounded by the large amount of each irregular-like single with the size of 105±4 nm, as shown in Figure 3f, and two sorts of the aggregated Pt particles Figure 3e, with a diameter of about 129±6 nm. The presence of such clots of Pt NPs might be due to the formation of assorted complicated formulas of

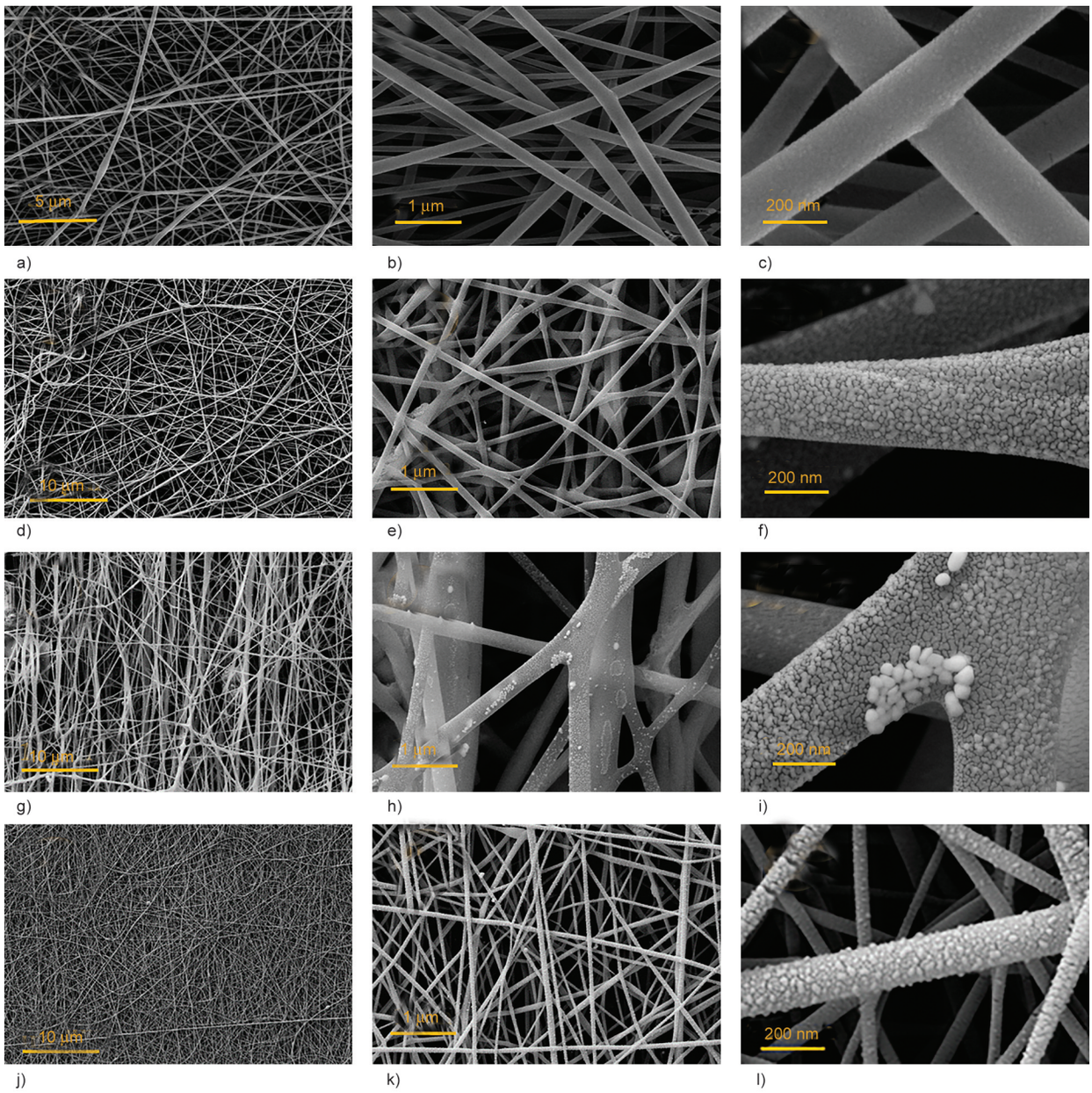

Figure 3. FESEM images of (a–c) pure PAN NFs, (d–f) Pt@ PAN, (g–i) Au@ PAN, and (j–l) Ag@ PAN NFs.

Pt ions [37]. Figures 3g–3i demonstrate the typical FESEM graphs of the Au NPs deposited over the PAN NFs. The size range of the quasi-spherical and polygonal shapes of Au NPs were 166±4 and 117±4 nm, respectively. Obviously, the PAN surface was covered with a uniform and compact layer of Au particles, which make distinctive fibers similar to a tree branch with scattered snowflakes on it, as shown in Figures 3h, 3i. It was found that the smallest-sized spherical Ag NPs were grouped alongside those massive particles along the fibers', as shown in Figures 3j–3l. TEM observations appeared unambiguous, as shown in Figures 4a, 4b, that the outer/inner PAN surface was pure before adding any metalized agent and had no irregularities and no beads. Virtues of immobilized Pt NPs and Pt@ PAN NFs were also measured via TEM images (Figures 4c, 4d) that both Clotted and polyhedral shapes of these particles were tangible. The structural deficiencies in this type of fiber gave a poor result for both mechanical properties and wettability. Figures 4e, 4f exhibit the TEM images of the as-spun Au@ PAN NFs. A close examination revealed that the Au NPs were loaded with different nanometer sizes and polygonal-shaped particles or spherical particles, which were separately scattered on their surfaces. In the same order, Figures 4g, 4h disclosed that Ag NPs have a spherical shape with good dispersion. From a morphological

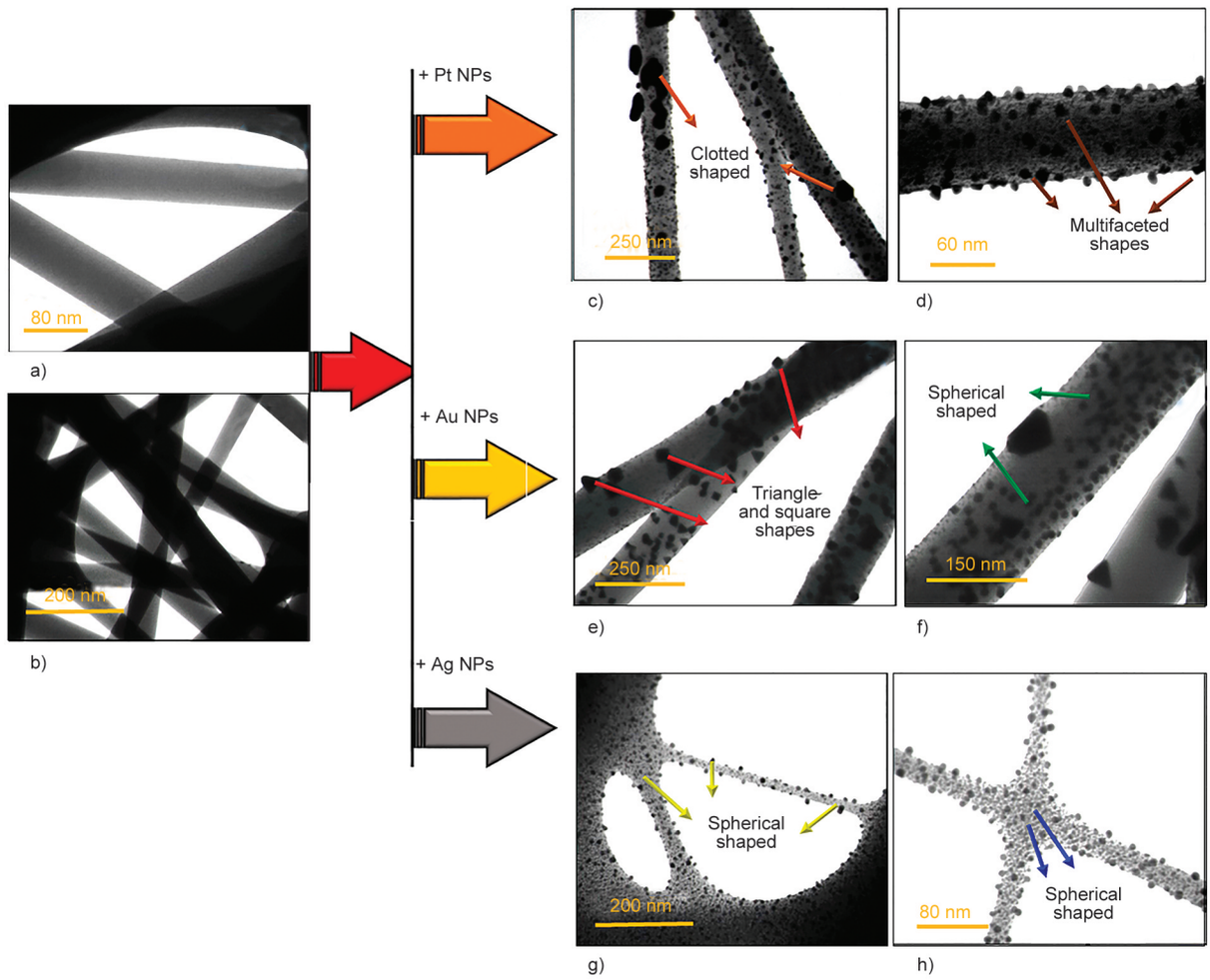

Figure 4. TEM images of (a, b) pure PAN NFs, (c, d) Pt@ PAN NFs, (e, f) Au@ PAN NFs, and (g, h) Ag@ PAN NFs.

study of all electrospun samples, some important notes can be extracted, as follows: (i) After adding the metalized reactants, it can be observed that not only the smoothness of PAN surface obviously vanished but also these metalized agents led to the remarkable enhancement in the average diameter of PAN NFs, according to the following order: PAN NFs < Ag@ PAN NFs < Pt@ PAN NFs < Au@ PAN NFs, because the size of loaded NM NPs increase in the same order Ag NPs < Pt NPs < Au NPs, as shown in Table 3. (ii) It may be noted, when reviewing the obtained results of *Z* values, a correlation that corroborates the validity of the outcomes of the morphological study. In the case of the homogeneous distribution of NM NPs, because of the largest interaction area with activated sites of the polymer surface, the formation of hydrogen bonds becomes better through the good, physically interlink between PAN and NM NPs thus, the *Z* values were also augmented, as reported in many papers [38]. On the other hand, the size of fiber diameter can be declined by enhancing the *Z* values, ascribing that the small generation diameter of fiber could be an outcome improvement of the molecular orientation chain

Table 3. Variations of loaded nanoparticles for many shapes and diameter fibers.

Sample	Sizes of loaded NPs [nm]	Average fiber diameter [nm]
PAN NFs	Bare of any loaded nanoparticles	268±3
Pt@ PAN NFs	129±6 'Accumulated particles' 105±4 'Irregular-like particles'	391±4
Au@ PAN NFs	166±4 'Quasi-spherical particle' 117±4 'Polygonal-shaped particles'	611±3
Ag@ PAN NFs	51±5 'Spherical particle'	311±4

along the fiber axis [39]. (iii) The detailed TEM results of samples discuss that the inner surface of fibers is more impregnated with NM NPs, particularly Ag NPs and Pt NPs, than their outer surface, due to strong links between NM NPs, most notably Ag NPs, and active sites containing nitrogen of polymer matrix [39].

3.3. Elemental analysis

The spectrum and the result of the quantitative analysis of PAN NFs, as shown in Figure 5a, exhibited the presence of carbon, nitrogen, and oxygen at different ratios and the absence of NM NPs. According to the EDX studies (Figure 5b–5d) and mapping images (Figures 6) of M@ PAN NFs, it clearly seems that the ratio of M(0) is close to the expected (10 wt%) based on the precursor compositions of the ES solutions. All SEM-mapping images explained the homogeneous distribution of all contents (Pt, Au, Ag, C, N, and O elements) over that related NFs. Moreover, this high amount of the metal NPs can be clarified by strong interaction between the electron pair of the nitrogen atom and the NM NPs [34]. The high content of C and N elements means that the interaction of particles with oxygen functional groups (carbonyl and hydroxyl) was lower than it was in the case of (–C=N) groups [40]. These analyses also provided good evidence that the fibers did not contain other impurities of metallic compounds such as Ag_2O, $PtCl_2$, $AuCl_3$, AuCl, etc. These behaviors are in good agreement with the XRD patterns.

3.4. AFM images

To detect more the structures of PAN NFs and M@ PAN NPs, the surface properties of these fibers were studied by the three-dimensional Atomic Force Microscopy (AFM) images, as shown in Figure 7a–7d and evaluated by JPK data processing software. According to these figures, it can be observed that the pristine PAN NFs, Figure 7a–7d, possess a much less

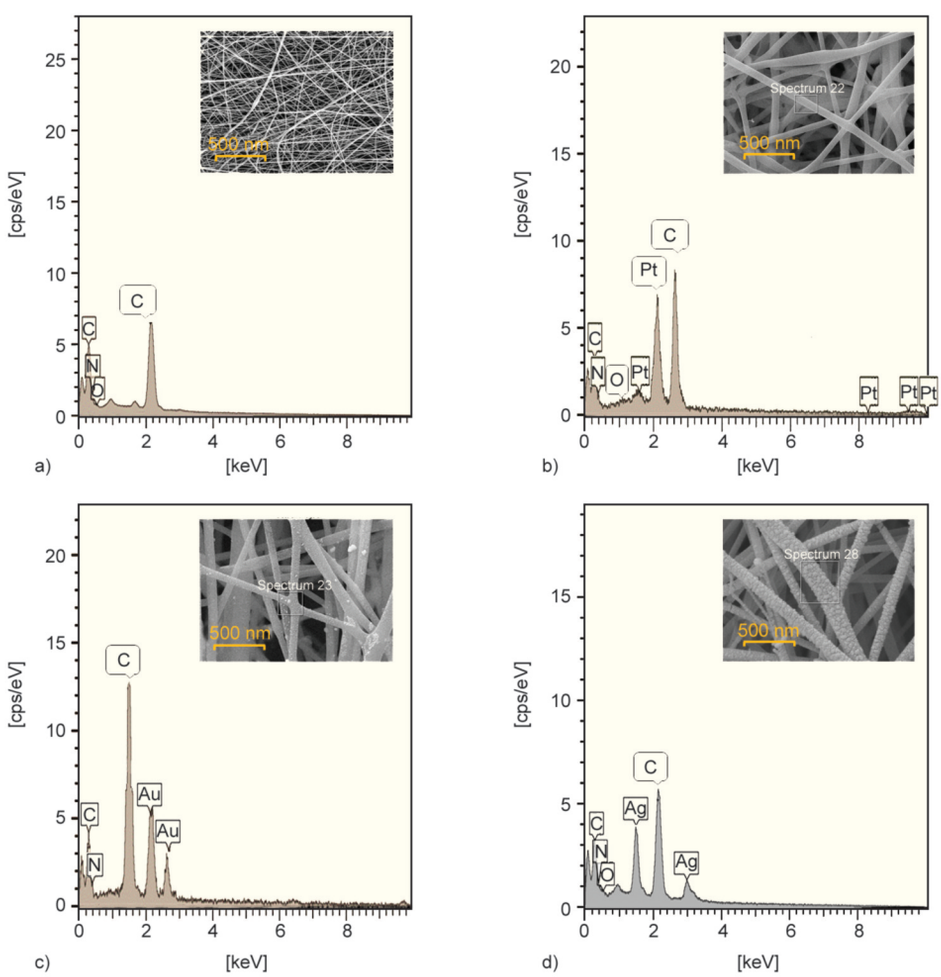

Figure 5. Area EDX spectra of (a) PAN NFs, (b) PAN NFs loaded with 10 wt% Pt NPs, (c) PAN NFs loaded with 10 wt% Au NPs, and (d) PAN NFs loaded with 10 wt% Ag NPs.

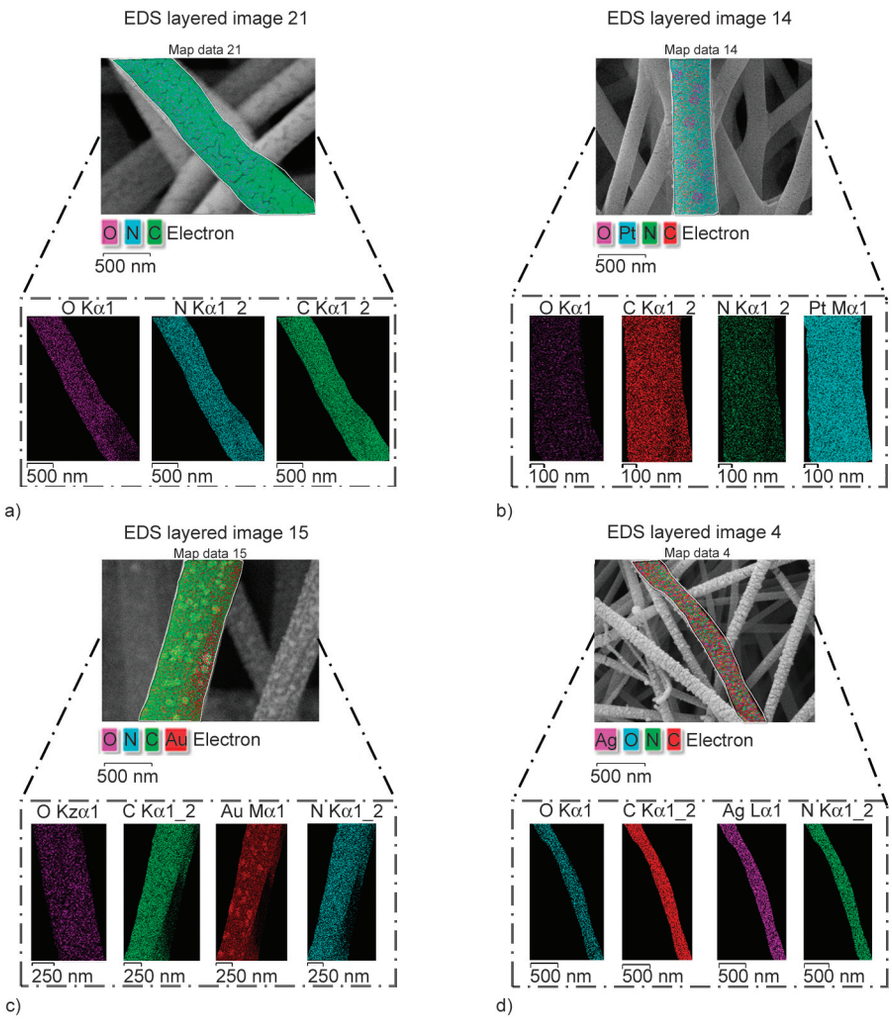

Figure 6. SEM-EDS elemental mapping of (a) (C, N, and O) for PAN NFs, (b) (Pt, C, N, and O) for Pt@ PAN NFs, (c) (Au, C, N, and O) for Au@ PAN NFs, and (d) (Ag, C, N, and O) for Ag@ PAN NFs.

rough surface than metalized PAN NFs. Comparing the 3-D AFM images of the PAN NFs Figure 7a–7d, the Pt@ PAN NFs (Figure 7b), and Ag@ PAN NFs (Figure 7d), the outer surfaces of Pt@ PAN NFs and Ag@ PAN NFs are a little rougher than the PAN NFs, because both these particles can be regularly immobilized on long external edges of the fiber polymers with fine distribution sizes. AFM topography images of Au@ PAN NFs are represented in Figure 7c. It is clearly evident that the Au@ PAN NFs have coarser surfaces than the corresponding pure PAN NFs and other metalized fibers. While the Au NPs were grown within the PAN NFs, others were assembled as islands on their external surface. The electrospun PAN NFs were relatively elongated and made fibers rather rough. Also, we believed that the underneath interaction of these particles with some part of the PAN surface contributed to the main elimination of the smoothness of the bare polymer. Average roughness (R_a) and Root mean square roughness (RMS, R_q) were also measured along ten single fibers in each case and averaged (Figure 7e). The statistical analysis of the results was performed using One-way ANOVA followed by Tukey's posttest. According to the results, both roughness parameters, R_a and R_q values were significantly higher in Au@ PAN NFs (P-value < 0.001) than those in Pt@ PAN NFs and Ag@ PAN NFs. There was no significant difference between the roughness parameters (R_a and R_q) of Pt@ PAN NFs and Ag@ PAN NFs (P-value > 0.05).

3.5. FT-IR study

The FT-IR technique was performed to prove the chemical structure of PAN NFs, the interaction between the added NM NPs and the functional groups on the surface of the PAN NFs, and shift in wavenumber after metallization in detail, and the results were fitted in Figure 8. FT-IR data of pure PAN NFs and their metalized NFs in the range (4000–400 cm^{-1})

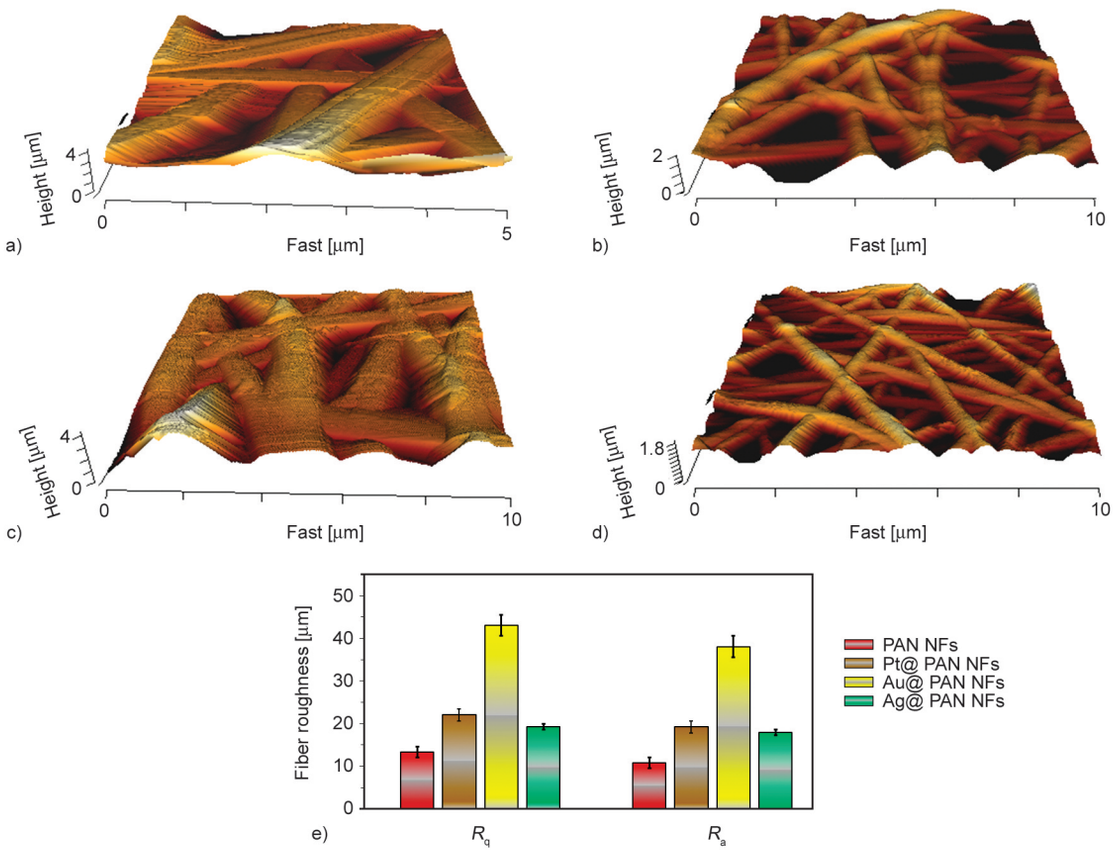

Figure 7. The 3-D AFM images of (a) PAN NFs, (b) Pt@ PAN NFs, (c) Au@ PAN NFs, (d) Ag@ PAN NFs and (e) comparison between R_a and R_q values the whole metalized fiber samples.

were summarized in Table 4. Also, the structural changes of the PAN NFs while its solution was heated at 75 °C in aerobic conditions were characterized through a comparison of FT-IR spectra of PAN powder that could help to predict the reactions at 75 °C. Figure 8a indicated the most significant differences in the intensity of (C≡N, C=O, C–H, C=N, C=C, N–H, O–H, C–CN, and C–N) functional groups and their locations for PAN NFs and PAN powder. The relevant spectrum of the PAN precursor powder disclosed characteristic IR-bands for several vibrations, including nitrile group (–C≡N at 2245 cm^{-1}), carboxylic acid groups (C=O at 536, 1646, 1732 cm^{-1} and C–O at 1237 cm^{-1}, which attributed to monomeric units of methyl acrylate, methyl methacrylate and itaconic acid [41, 42] with a weak or medium intensity) aliphatic groups (δ_{C-H} at 2949 and 1359 cm^{-1}, ν_{C-H} at 1455 cm^{-1} and C–C at 1070 and 1251 cm^{-1}) and mixed modes (O–H + N–H at a range of 3100–3700 cm^{-1}) [41, 43]. It can be observed from Figure 8a that the vibrations (–C≡N, C=O, C–O, δ_{C-H}, ν_{C-H}, (O–H + N–H) and C–C) of PAN NFs were located at 2245, 2342, 539, 1666, 1236, 1455, 2949, 1386, range of (3100–3700, as a broad peak) and 1076 cm^{-1}, respectively. [24, 41, 44]. The same figure indicated the appearance of a sharp peak at the region of 1580–1720 cm^{-1}, which this peak was composed of multi overlapping peaks (marked with a circle, Figure 8a). This observation was in good agreement with Dang's paper [44]. The spectral report of these multi overlapping peaks of PAN NFs was given in below [41–44]:

Spectral report: peak located at 1595, 1652 cm^{-1} (C=N) (shoulder), 1600 cm^{-1} $(C=N)_n$, 1660–1690 cm^{-1} (C=O), 1580–1655 cm^{-1} (C=C + C=N), 1600 cm^{-1} (ν_{C-N} + $\nu_{C=N}$ + δ_{N-H}), 1716 cm^{-1} (C=O in cyclized structure of polymeric matrix) (shoulder).

As shown in the spectrum (Figure 8a), related to PAN NFs, the IR-bands were observed at 2242 and 2327 cm^{-1} with medium and weak intensity, respectively, due to the existence of C≡N stretching vibration in the isolated and short units of ($–CH_2CHCN–$) form [26, 29]. The gradual profit of the intensity peak at 1595, 1652, 1600 cm^{-1} corresponded with the C=N, C–N, and (C=N)n groups, and the gradual loss of the intensity peak at 2244 cm^{-1}, corresponding to the C≡N groups, can be suggested that the (–C≡N) groups can be converted to the (–C=N)

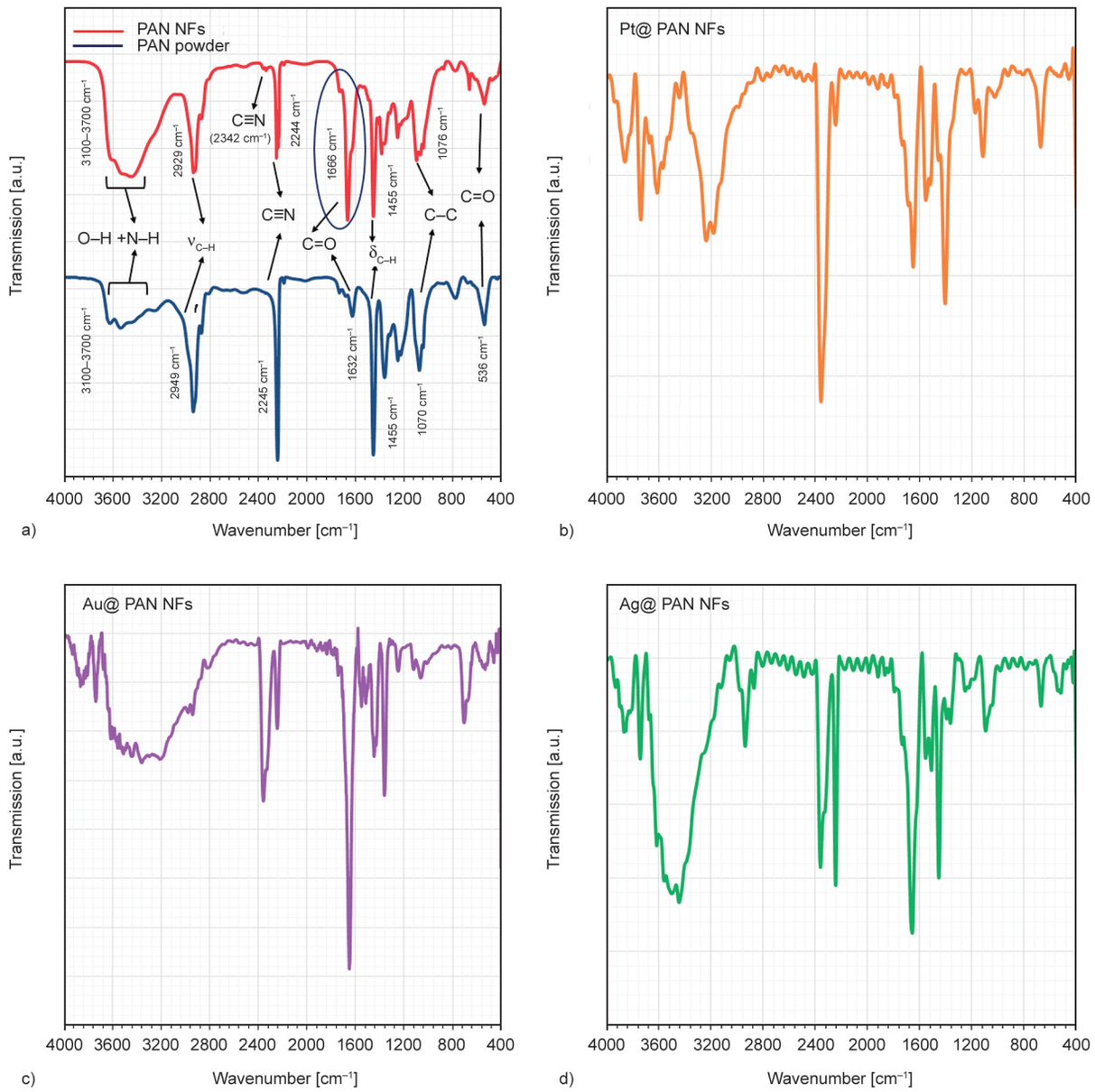

Figure 8. FT-IR spectra of (a) PAN powder and PAN NFs, (b) Pt@ PAN NFs, (c) Au@ PAN NFs and (d) Ag@ PAN NFs.

groups, due to transformation in the PAN structure (from linear to ring structure) by cyclization and dehydration reactions under [25, 43]. On the other hand, the intensity of IR-band around 1666–1690 cm^{-1} (for PAN NFs) was more than the intensity of IR-band around 1629 cm^{-1} (for PAN powder) that shifts towards a larger wavenumber due to the formation of a stable cyclized structure of polymeric matrix under the aerobic condition with progress in cyclization reaction [4, 18]. The process of converting a linear PAN structure into cyclized (or ladder) structure has been extensively investigated [45–49]. Many papers have described the heating of PAN solution in the atmosphere at low temperatures [31, 43, 50]. The transformation mechanism of the linear PAN structure to its cyclized structure assumed that the transformation was carried out by dehydrogenation path rather than the cyclization path under heating-treatment of PAN solution in aerobic conditions, which was previously reported by Karbownik *et al.* [43]. Based on their FT-IR results, the presence of the system of the C=C, C=N oscillations in the final fibrous product proved the formation of the hexagonal rings of PAN under the applied conditions [43]. Park *et al.* [31] exhibited dissected that the reason for the appearance of efficacious oxygen collections like (ketones, hydroxyls, *etc.*) over the PAN surface was back to the heating-oxidation of polymer for a prolonged time at 100 centigrade under air that has been confirmed by the ESR and FTIR analyzes.

According to Park's results, some critical interactions such as intra-molecular interactions and hydrogen bonds within the compound were generated. As a result, the aromatic structures of the polymeric matrix were partially formed by the dehydrogenation reaction [27]. According to these studies of Karbownik *et al*. [43], Wang *et al*. [51], and Park *et al*. [31], it can be suggested that it is possible to obtain a ring structure of PAN by heating at low temperature in the presence of oxygen. Therefore, it is necessary to mention the role of oxygen in the transformation process. As stated in Friedlander's explanations, this cyclized structure, as-called naphtyridine-type ring, can absorb oxygen easily to form units with an oxygen content (polynitron units) [30]. Park showed in his study that the oxygen groups in the comonomers like methyl acrylate and methyl methacrylate groups were as activated centers to start the cyclization process of polymeric matrix by the nucleophilic or electrophilic attack of the carbon of the C≡N groups [31]. The limited amount of oxygen in the atmosphere with heating positively affects the acceleration of the transformation reaction and stabilization of the structure of the polymeric matrix [28, 44]. As confirmed by our FT-IR analysis of PAN NFs, in which its electrospinning solution was heated for 18 h at 75 °C, the presence of combination vibrations of C=C, C=N, C–N with oxygen groups such as C=O, O–H, C–H, and C–N in the polymeric matrix backbone allowed to provide more stability of the related fibers by the creation of some of the critical interactions such as intra-molecular interactions and hydrogen bonds of the polymeric matrix chain such as (OH…OH, CN…HO, *etc*.) [42, 46]. Formation of the conjugated system of $(C=N)_n$ (as a Chromophore unites), formation of random copolymers such as polyimine and polynitron system during oxidation pathway, the presence of acidic comonomers- which promotes ionic mechanism of the converting structure of PAN and it can help for forming of a chromophore center of C=C, and strong intramolecular cross-linking. This is a significant reason to prove the occurrence of the changes in the color of polymeric solution (see digital images in Figure 1, Step 2) [24–31].

The FT-IR spectra (Figure 8b–8d) of Pt@ PAN NFs, Au@ PAN NFs, and Ag@ PAN NFs are not only similar to that of pure PAN NFs, but also some of the unorthodox changes in their corresponding wavenumber are monitored. From reported spectra (Figure 8b–8d), the intensity of (–C≡N) group (at 2242 cm^{-1}) and the intensity of (–C=N) group (at 1652, 1593, and 1668 cm^{-1}) were articulately changed, indicating a constrict number of the –C≡N groups after reacting with metalized agents. More precisely noting in Table 4, the vibrational of two former bands shifted towards higher and lower wavenumbers together due to anisotropy virtues of lattice dilatation of fine particles [52]. Compared with PAN NFs, the C=O peak shifted to a higher wavenumber from 1610 to 1623–1631 cm^{-1} of NM@ PAN NFs. According to former observations, it is implied that the interaction between NM NPs and partial donation of nitrogen (in –C=N groups) and oxygen (in –C=O or –OH groups) loan pair electrons of PAN molecules may occur more frequently [53]. The surficial absorption and the hydrogenous bonds of metalized agents at the low nanoscale were stronger than other ones at the high nanoscale, indicating that the noticeable wavenumber shift in the large absorption regions was more detectable which have signalized by Matsumura *et al*. [53]. Before comprehending the final explanation of this section, two questions have arisen: how did these metallic reinforcements affect the stability structure of fibers? And what is their role during the preparation

Table 4. Brief of main peaks of FT-IR spectra of PAN NFs and whole as-prepared metal @PAN NFs [cm^{-1}].

Functional groups	PAN NFs	Pt@ PAN NFs	Au@ PAN NFs	Ag@ PAN NFs
–C≡N	2244 ■ 2327 ●	2221 ● 2350 ■	2223 ■ 2360 ■	2230 ● 2365 ■
–C=N	1593 ● 1580 ▲ 1653 ●	1512 ■ 1550 ■ 1638 ■	1514 ● 1546 ■ 1640 ■	1520 ■ 1562 ■ 1650 ■
–C=O	1610 ●	1623 ■	1627 ■	1631 ■
–N–H	3614 ▲	3618 ■	3614 ■	3620 ■

▲ High-intensity
■ Medium intensity
● Low intensity

of electrospun solution? To answer these questions, the relative cyclization rate (*RCR*), as an indicator of the formation of the cyclized structure of PAN via dehydrogenation and cyclization reactions, using the FTIR spectra, as given in Equation (3), was evaluated for all as-prepared polymeric fibers (before and after adding the metalized agents). The obtained *RCR* values were 49.80% for PAN NFs, 49.78% for Pt@ PAN NFs, 50.41% for Au@ PAN NFs, and 51.23% for Ag@ PAN NFs (see Figure 12a in 3.8. section). The metalized agents accelerated the formation of an arranged cyclized regulation consisting of the chemical band (C=C=N). Thereby, it is concluded the metalized agents participated in the strengthening of the formed chemical bonds between the functional groups in the polymeric chains and improvement of the polymeric chain stability during the heating-oxidation of the polymer solution.

3.6. Study of mechanical property

In Figure 9, the strain-stress curve is sketched for PAN NFs and for the three types of metalized fiber specimens, while more detailed information of the variation of the calculated mechanical parameters (σ, $\ddot{Y}$ and $\dot{E}$) for all fiber groups are presented concisely in Figure 12 (σ, $\ddot{Y}$, and $\ddot{E}$, as the indicators of the mechanical properties) As mentioned to the same figure (Figure 9), the values of σ, $\ddot{Y}$, and $\ddot{E}$ for the corresponded samples are augmented with the increment the content of NM NPs to 10 wt%. From the related figure (Figure 9), the σ values of Pt@ PAN NFs, Au@ PAN NFs, and Ag@ PAN NFs are about 1.074±0.034, 1.907±0.071, and 2.367±0.065 MPa, respectively and the $\ddot{Y}$ values are 0.29, 0.56, and 0.76 MPa. The breakage elongation had an ascending trend, which is reached 3.378% for Pt@ PAN NFs, 5.737% for Au@ PAN NFs, and 6.368% for

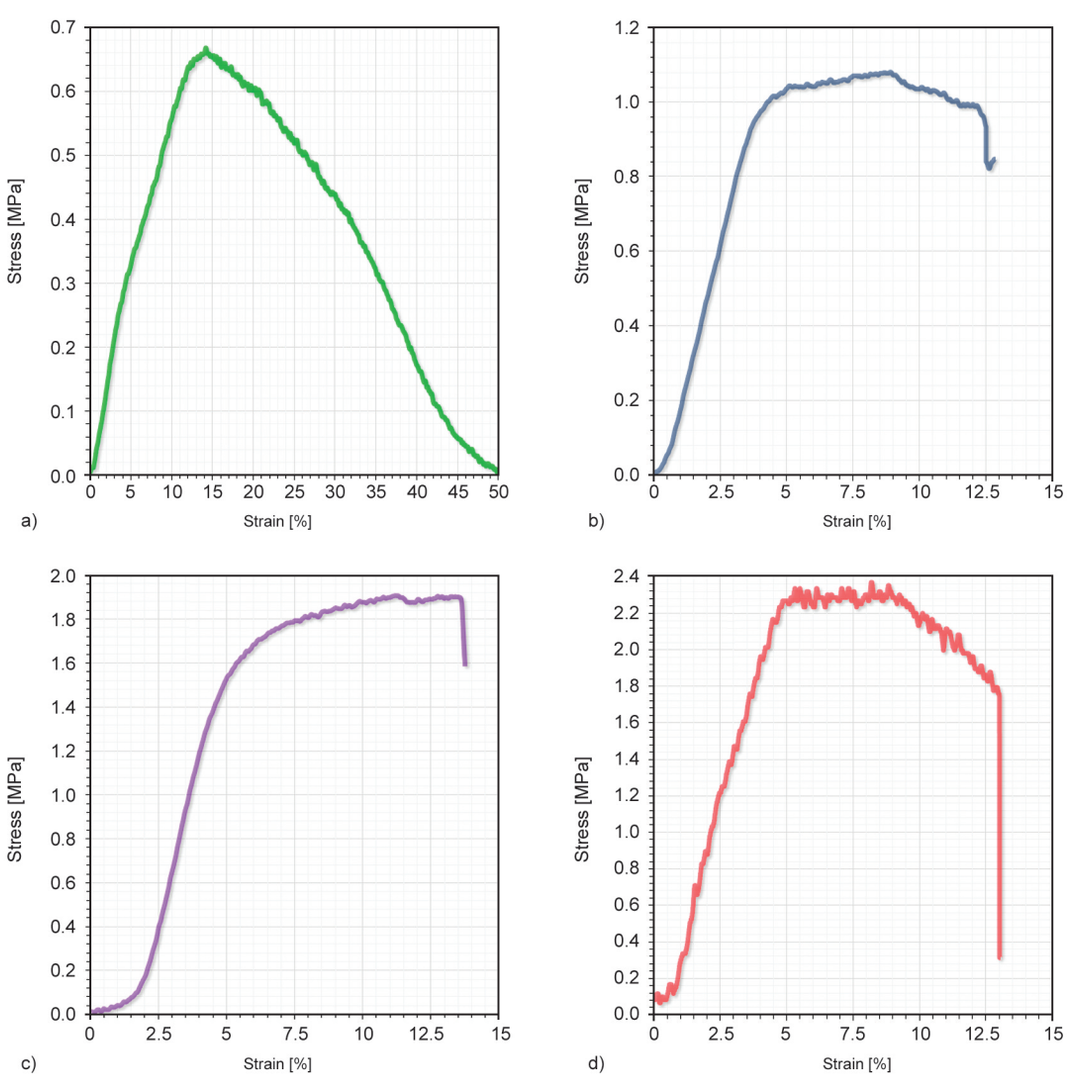

Figure 9. Tensile stress-strain curves of (a) PAN NFs, (b) Pt@ PAN NFs, (c) Au@ PAN NFs and (d) Ag@ PAN NFs.

Ag@ PAN NFs. The PAN NFs possess σ and $\ddot{Y}$ of 0.611 and 0.71 MPa, respectively, at 7.336% elongation. The extracted results from the previous data are debated for some critical reasons, *i.e*., the size of nanoparticles and their architectures, fiber diameters, and degree of crystallinity [54]. As a final result, increased σ (superior strength) and increased $\dot{E}$ (large ductility) of samples can be interpreted by the presence of metalized species with good crystallinity and uniform dispersion. By using the theory of the energy-dissipation mechanism [54], the orientated and aligned nanoparticles provided additional energy centers to reinforce the mechanism interlocking during the creation of temporary decussated adhesions among fibers. Metallic reinforcements act as restrictors to prevent sudden dislocations of the polymeric matrix in this step. The concentration of agglomerated disturbances and the obvious enhancement of the tensile stress are considered as initial points for the up-growth of micro-cracks, fractures, and interfacial debonding between PAN matrix and loaded particles [54]. The effect size of the M NPs on the mechanical factors of the resulting metalized fibers is addressed from two significant axes. First, the tensile forces are orderly distributed at each point of the fiber with the decrease in the size of NPs. Second, such outstanding mechanical parameters could benefit from mechanical percolation influence between the inner PAN surface filled with the small size of the metallic particle and from the strong interactions between metallic particles themselves, both promoting the formation of rigid interconnected mesh structure to resist the tensile process and to improve its corresponding parameters [54]. In the case of large-sized particles (particularly Pt NPs and Au NPs), as confirmed in FESEM images (Figure 3e, 3i), the tensile forces are concentrated on the weak boundary area between that particles and PAN, so the prevalence was uneven along with the relevant fiber. That being so, the large-scale of loaded Pt and Au particles provide the low mechanical values of their corresponding nanofibers [54]. The leverage of the shape of M NPs can be explained as follows: the arranged spherical shape of Ag particles gave a better answer to the diffuse mechanical forces because their movement is well-arranged under applying tensile stress. The many facets of the polygonal shapes of both Au NPs and Pt NPs, its heterogeneous distribution over or inside surface the fibers, and the difference in the magnitude of the tensile forces around each point of the polygons can be considered as clear indicators for the low mechanical properties of each their fibers.

3.7. Assessment of the wettability measurement

Figure 10 displays a presentation of the wettability property and retaining it on the PAN NFs surface before and after their metallization process and the *WCA* values at multi times (10, 20, and 30 sec.) for each of them. Note that with further retaining time of the water droplets on the surface of the as-prepared NFs, the *WCA* somehow went down. This is due to the long-termed heat treatment, which led to the formation of the abundant content of polar parts (hydroxyl, carbonyl, and nitrogen groups) and at the same time played a key role in the migration of the non-polar components from the inner part of the polymeric matrix to its outer part [55, 56]. It is allowed to decrease the polarity of the PAN NFs and to form a slightly weaker hydrogen bonding with water molecules, compared to the polar surfaces [55, 56]. Thereby, the PAN NFs have a good hydrophilic surface with a *WCA* value of 24.23° after 30 seconds. After metallization with Pt NPs and Au NPs, it is noticeable that the *WCA* was large in both cases. It decreased slightly with the increasing retaining time, compared to the *WCA* of non-metalized polymer fiber or Ag@ PAN NFs, due to the modification of the nature of the PAN NFs by many sizes of the NM NPs.

3.8. The physiochemical structures and (structure-properties) relations

3.8.1. The (chemical structure-crystal structure) amd (morphology-crystal structure) relations

The results of the crystalline study (3.1. section) indicated a clear change in the degree of crystallinity and the scale of crystals of PAN after the metallization process. Here in this section, we explain the effect of the process on the PAN NFs by studying the correlation of (*Z vs*. *RCR*) and (*Z vs*. (particles sizes and fibers diameters)). As shown in Figure 11, the *RCR* of M@ PAN NFs increased with the increase of the *Z*%. The small nano-size and good dispersion of the Ag NPs induced the orientation of the PAN molecular chains around the surface of Ag NPs, which was closely belonged to the expansion of the *Z*% values of PAN (as compared to rest metalized PAN NFs). At the same time, the PAN fibers metalized in Ag NPs

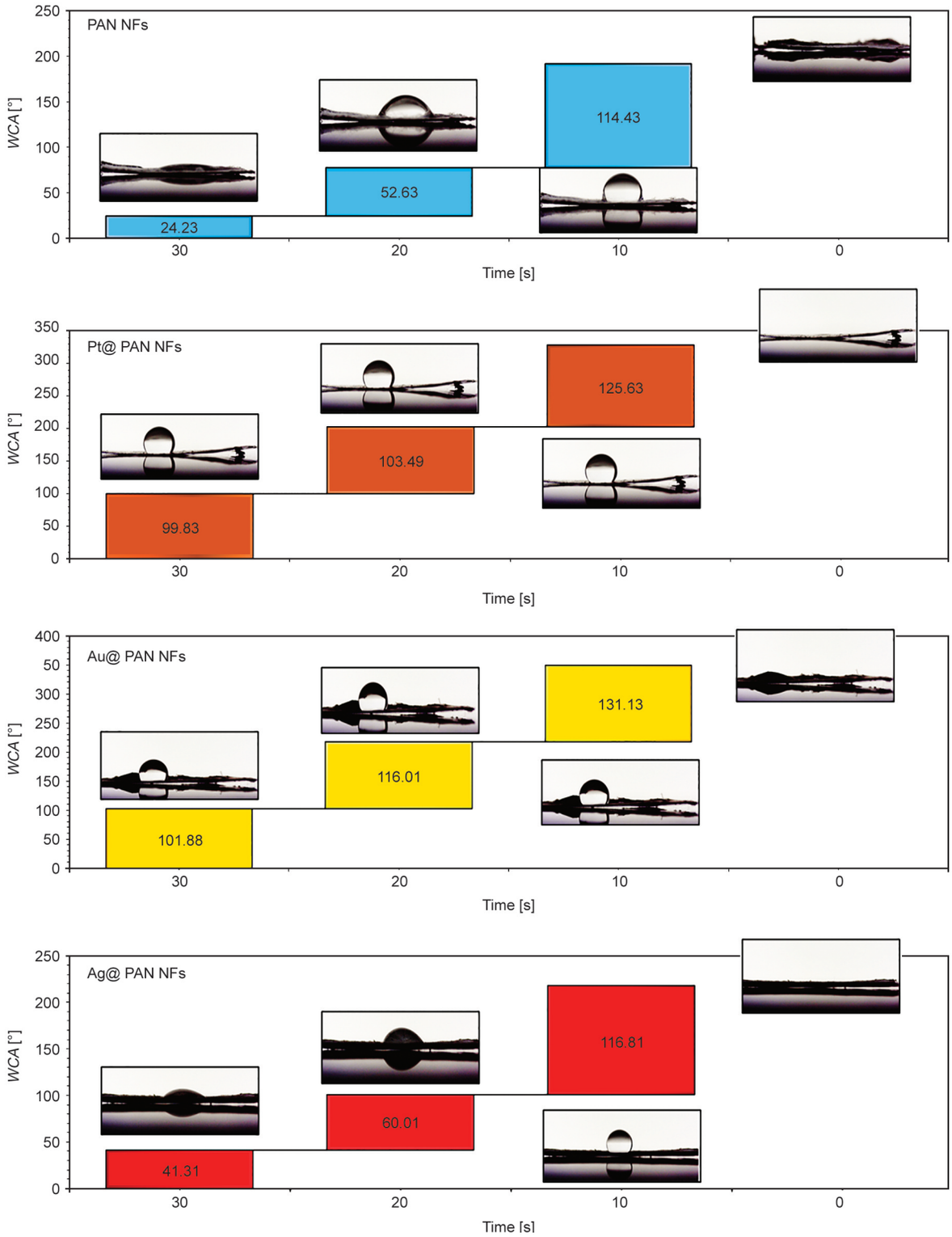

Figure 10. The variation of *WCA* of the whole as-prepared fibers at different times and at different magnifications with the digital photo of water drops on their surfaces.

had more stabilized and cyclized than the other fibers metalized in the same condition of temperature and electrospinning, indicating the higher level of the cyclization and dehydrogenation reactions (the high *RCR* value). The *RCR* results, together with the results of FTIR and the XRD, tell us that the upgrowth of a large number of the vigorous linkers in the cross-network of the polymeric structures and the production of stronger interconnections in the polymer chains at higher *RCR* corresponded with a change in the rate of crystallization of the PAN in the M@ PAN NFs as compared to its pure state. As it is

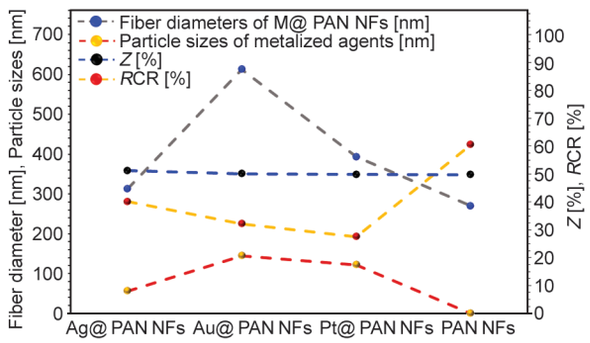

Figure 11. The effect of the variation of the (*Z*%) values on *RCR* [%] values and on the dimensions of the loaded NM NPs and on the size of the diameters of the fabricated fibrous structures.

known that metals, in general, are thermally resistant materials, so in fact, the added metallic particles play like carriers for the heat generated by the cyclization and dehydrogenation reactions, which is to say, the metalized agents lessen the temperature of those reactions to gain metalized PAN NFs with the best cyclization level [25]. The related figure showed that there was a direct relationship between the morphological properties (represented by the size of the metalized agents and the diameter of the polymeric fibrous structure) and the degree of crystallization as well. As an obvious consequence of this direct relation, the *Z*% change of PAN in the M@ PAN NFs was associated with an increase in the diameter of the M@ PAN NFs and nanoscale of metalized agent particles. The abundant presence of functional groups, symmetrically immersion and deposition of metalized agents (less nanoscale then larger) in/on the inner and outer surface of the PAN NFs and no increase in structural defects of the polymeric matrix gave a noticeable modification in the orientation of the PAN at the common boundary with the NM NPs and resulted in a marked difference in fiber diameters with modifications in *Z*%, in good agreement with Huan *et al.* [57] (see FESEM and TEM micrographs).

3.8.2. (Engineering properties and structural features of metalized fibers) relation

The (variation of tensile parameters *vs*. variation of structural properties) curve of the different as-prepared nanofibers is displayed in Figure 12a. Firstly, the results obtained, shown in the summary of the correlation of mechanical test results with morphologies of NM NPs and fibers, a significant increase in the values of σ, $\dot{Y}$, and $\ddot{E}$ with the loss in size of metalized agents and the loss in diameter for M@ PAN NFs. According to mechanical percolation influence [54], these increments were due to the various stiffness interactions promoted by the small size of the particles compared to larger sizes of the particles. In addition, the large size of metalized agents, the coagulate shapes, and their dispersion in the PAN are considered inhibitors to the transfer of tensile forces along the fibers. The experimental data indicated that the M@ PAN NFs laminates with the high content of crystals and with the smallest size of diameter displayed higher mechanical parameters, suggesting that a strengthening of the interfacial bonding was occurred as well as improved the NFs. Unlike Ag@ PAN NFs, a decreasing trend was predestined for σ, $\dot{Y}$ and $\ddot{E}$ values, as the increasing

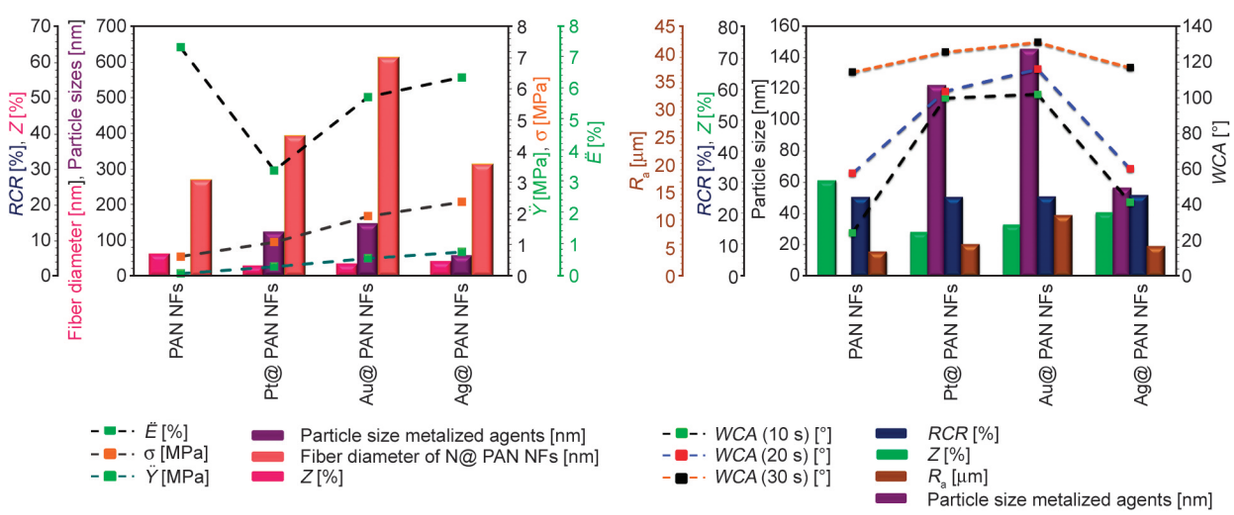

Figure 12. The correlations between structural physiochemical parameters for as-synthesized fibers and (a) engineering properties (b) wetting properties.

of fiber diameter, in other two electrospun nanofibers (Au@ PAN NFs and Pt@ PAN NFs). This behavior is because the alignment and re-orientated of fiber lamellae structure were decreased with the increment diameter of former fibers [58]. On the other hand, the fine fibers with the narrow distribution of particles help increase the value of $\ddot{Y}$ and σ because a large number of fine fibers and particles participate in the tensile process [58]. Based on the crystal studies, one can notice that the *Z*% of all electrospun metalized nanofibers could be responsible for improved mechanical parameters. It was found that the addition of metallic components allowed an increase in the degree of crystallinity and molecular orientation of the fibrillary structure of each sample. Therefore, the Pt@ PAN NFs, which were fabricated with low *Z*% and structural defects, have the least resistance under any certain stress, resulting in small tensile strength and elongation.

3.8.3. The (Wetting properties amd structural features of metalized fibers) relation

Figure 12b depicts the correlation between variation in the values of *WCA* at different times with variation of the physicochemical properties (*RCR*, Z%, particle size, and R_a). From the obtained data, we hypothesize that these interesting results are closely linked to the mechanism of changing the chemical composition of the metalized fibril structure that is discussed briefly by following reasons. The first reason, based on the previous interpretations (high *RCR* rate and *Z*%, section 3.8.1), is that increasing both parameters lead to the formation of fibrous surfaces with stable structures. Through this, it is known that the crystal structures of metallic compounds are nonpolar and, therefore, the presence of them on the surface of the polymeric fiber reduces its polarity [55, 56]. This means that the hydrogen bonds formed with water molecules are rather weak. Therefore, it was noted that the contact angle was greater than in the case of the bare fiber (PAN NFs) (deterioration in the hydrophilic property) [55]. It can also be explained that the weak interaction of the aggregated particles (particularly for Pt NPs and Au NPs) with the polymer surface mainly affects the reduction of the interfacial free energy of the fibrous surfaces (also no improvement of the *WCA*s) [55, 59]. Third, the relationship (surface roughness/contact angle) directly affects the hydrophilicity of the metalized nanofibers. Stacking the coarse fiber layers in Au@ PAN NFs and Pt@ PAN NFs, having Au NPs and Pt NPs in different shapes and sizes respectively, on top of each other leads to create the formation of air pockets between these coarse layers, plateaus, and ridges, therefore, these two types of metalized nanofibers did not possess sufficient surface area for water droplets to contact their surfaces [55]. When the number of agglomerated Pt NPs and Au NPs were loaded on the polymeric matrix, the surface-to-volume ratio of the related fibrous structures is reduced, and the diameter of the fibers is increased. These results could serve as key cues for an apparent decrease in the *WCA* values and reduction in hydrophilicity of the former nanofibers. Quite in contrast, the coordinated scattering of Ag NPs in/on PAN NFs, lower R_a values and high surface area of Ag@ PAN NFs, and their small diameter accelerate the permeability of water droplets and reduce *WCA* values [55, 59]. This disclosed the wettability surface difference ween NM@ PAN NFs and PAN NFs, due to changing the structural properties of it.

3.8.4. The synergistic relation (Wetting properties and mechanical properties)

Figure 13 shows the synergistic relationship of *WCA* change with the mechanical properties of the as-prepared fibers. It was also shown in the section of studying the mechanical properties (3.6. section) and the relationship (structural synergy/mechanical properties) section (3.8.3. section) that the good dispersion of metalized agents, especially Ag NPs with small sizes compared to gold and platinum particles, significantly improved the mechanical properties of

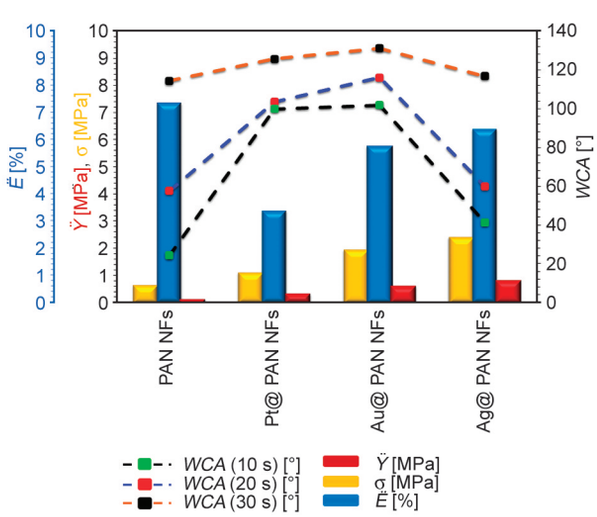

Figure 13. The synergistic relationship between the mechanical properties and wettability of all as-synthesized nanofibers.

the polymeric matrix. The small size particles not only changed the orientation of the polymeric chain but also contributed to increasing its rigidity by forming more robust bonds between polymeric matrix and metalized agents. In contrast to the case of larger-scale particles, the mechanical properties of the polymeric matrix were less improved because they contributed less to the increase in the rigidity of the polymeric matrix. In other words, as Rahmani pointed out [60], the flexibility, as a mechanical property, of the polymeric matric chains is the most influential factor on the hydrophilic properties. The rigidity of the polymeric surface decreases the wettability with the increase in the mechanical rigidity because this increase in rigidity does not allow the polar groups to easily penetrate the water into the surface of the polymeric matrix [60–62]. The other influencing factor is the change of surface energy while changing the rigidity of the fibrous structure. The most plausible reason from an energy point of view is that a more rigid structure (in the case of Ag@ PAN) will have lower surface energy, and as a consequence, the *WCA* is reduced, compared to the rest of the N M@ PAN NFs.

4. Conclusions

In this paper, we reported a consistent theoretical and experimental survey of the metallization of the PAN polymer matrix with three types of NM NPs (Pt NPs, Au NPs, and Ag NPs) and examined their effect on their mechanical properties and surface wettability. Based on the above findings and discussion, a summary of the main conclusions can be introduced as below:

(1) New series of metalized polymeric nanofibers (Pt@ PAN NFs, Au@ PAN NFs, and Ag@ PAN NFs) were successfully synthesized by combining two routes (electrospinning and ultrasound ways) sequentially and simultaneously as a one-pot reaction. At the first step, distinctive morphologies with good crystallinity of Pt, Au, and Ag NPs with (1 1 1) facets, as dominant planes, were fabricated by reducing the reaction using ($DMF/N_2H_4{\cdot}H_2O$) in the presence of ultrasound irradiation. A green and easy character was conferred to the polymer solution preparation step by heating in aerobic conditions that involve the formation of a cyclized structure (–C=N, of PAN by the reduction of the nitrile groups (from C≡N to C=N) and creation of polar functionalized groups (–C=O, –OH) at 75 °C. By studying the morphology of the fiber surface, it was determined that the types and shapes of the smaller range of M NPs were loaded on the surface of PAN fiber, whereas the larger ones were located on its external surface. The diameters of the nanofibers were changed unspectacularly and this change was dependent on the type and shape of the metallic agent particles. The obtained AFM data (3-D images, average roughness (R_a), and Root mean square roughness (RMS, R_q) values) of the metalized nanofibers (NM@ PAN NFs) affirmed that the Au@ PAN NFs surface was more coarseness than others.

(2) The addition of metalized agents (as primary nucleation agents) is a positive influence in changing the physical properties of the PAN NFs. With the addition of such agents, all the crystalline properties of the PAN NFs were dramatically changed, depending on their types, shapes, and scales. On one hand, the change of *Z*%, in turn, affected the diameter of the fibers by changing the molecular orientation of PAN and on the particle distribution by forming hydrogen bonds with functional groups in PAN. FTIR analysis indicated that the metallic additives and PAN NFs were physically interconnected, which led to a good distribution of M NPs on electrospun fibers. The strength of this interconnection was governed by the charge density of the functional group and its ability to form strong physical bonds with the metalized agent, in addition to that, the emergency change in the average shift in the wavenumbers, after metallization, was also related to the size and shape of the metal particles. Another positive contribution of the metallic agents was the augmentation of the stability of the cyclic polymer structure after heat treatment at 75 °C, which was proven by calculating the *RCR*%.

(3) The difference between the tensile strength of PAN NFs and NM@ PAN NFs was examined using a tensile test machine. A modification of poor mechanical properties of PAN NFs can be observed after the loading of M NPs. In this test, the NM@ PAN NFs had higher mechanical modulus compared with electrospun PAN NFs that is due to the formation of the rigid interconnected network and mechanical percolation effect in (PAN chains/metalized agents) couple, making

elevation of the resistance vis. the tensile forces. In addition to what was indicated, the values of the ultimate tensile strength, Young's modulus, and elongation at break were greatly influenced by the synergy between metalized nanofibers morphology, particle size, and *Z*%. Considering all cases, it was found that the mechanical responses of both fiber's small diameter with either external edges or internal surfaces supported by small spherical particles are better than those of larger diameters and loaded with coagulated particles. This observation back to increment the *Z*% and molecular orientation with the depreciation of size particles.

(4) Wettability measurements depicted the *WCA* values of the bare PAN NFs is low (*WCA* = 24.23°) at 30 sec, confirming a good hydrophilic surface. Interestingly, the *WCA* of Ag@ PAN NFs decreased from 116.81 to 41.31° with increasing retaining time of the water droplets on its surface, indicating a good hydrophilic character. But, the *WCA* for Au@ PAN NFs and Pt@ PAN NFs also slightly decreased from 131.13 to 101.88 and 125.63 and 99.88°, respectively, suggesting hydrophobic. The wettability property was also affected by the structural synergy of R_a, *RCR*, and *Z*%.

(5) More importantly, there is a good synergistic correlation between the wettability property and the mechanical properties of the as-prepared fibers.

Acknowledgements

We gratefully acknowledge the Iran University of Science and Technology and Stem Cell Technology Research Center for providing materials and facilities.

References

[1] Sivasankarapillai V. S., Das S. S., Sabir F., Sundaramahalingam M. A., Colmenares J. C., Prasannakumar S., Rajan M., Rahdar A., Kyzas G. Z.: Progress in natural polymer engineered biomaterials for transdermal drug delivery systems. Materials Today Chemistry, **19**, 100382 (2021). https://doi.org/10.1016/j.mtchem.2020.100382

[2] Kim P., Epstein A. K., Khan M., Zarzar L. D., Lipomi D. J., Whitesides G. M., Aizenberg J.: Structural transformation by electrodeposition on patterned substrates (STEPS): A new versatile nanofabrication method. Nano Letters, **12**, 527–533 (2012). https://doi.org/10.1021/nl200426g

[3] Sung J., So H.: 3D printing-assisted fabrication of microgrid patterns for flexible antiadhesive polymer surfaces. Surfaces and Interfaces, **23**, 100935 (2021). https://doi.org/10.1016/j.surfin.2021.100935

[4] Lu X., Wang C., Wei Y.: One-dimensional composite nanomaterials: Synthesis by electrospinning and their applications. Small, **5**, 2349–2370 (2009). https://doi.org/10.1002/smll.200900445

[5] Zaarour B., Zhu L., Huang C., Jin X.: A mini review on the generation of crimped ultrathin fibers *via* electrospinning: Materials, strategies, and applications. Polymer for Advanced Technologies, **31**, 1449–1462 (2020). https://doi.org/10.1002/pat.4876

[6] Zaarour B., Zhu L., Jin X.: A review on the secondary surface morphology of electrospun nanofibers: Formation mechanisms, characterizations, and applications. Chemistry Select, **5**, 1335–1348 (2020). https://doi.org/10.1002/slct.201903981

[7] Zheng Z., Zhang Y., Yi F., Chen C., Song X.: Surface metallization of alumina ceramics: Effects of sintering time and substrate etching. Ceramic International, **40**, 12709–12715 (2014). https://doi.org/10.1016/j.ceramint.2014.04.119

[8] Drakopoulos S. X., Psarras G. C., Ronca S.: Oriented ultra-high molecular weight polyethylene/gold nanocomposites: Electrical conductivity and chain entanglement dynamics. Express Polymer Letters, **15**, 492–502 (2021). https://doi.org/10.3144/expresspolymlett.2021.42

[9] Abe M. M., Martins J. R., Sanvezzo P. B., Macedo J. V., Branciforti M. C., Halley P., Botaro V. R., Brienzo M.: Advantages and disadvantages of bioplastics production from starch and lignocellulosic components. Polymers, **13**, 2484 (2021). https://doi.org/10.3390/polym13152484

[10] Jamkhande P. G., Ghule N. W., Bamer A. H., Kalaskar M. G.: Metal nanoparticles synthesis: An overview on methods of preparation, advantages and disadvantages, and applications. Journal of Drug Delivery Science and Technology, **53**, 101174 (2019). https://doi.org/10.1016/j.jddst.2019.101174

[11] Mittal K. L.: Adhesion aspects of metallization of organic polymer surfaces. Journal of Vacuum Science and Technology A, **13**, 19–25 (1976). https://doi.org/10.1116/1.568850

[12] Shacham-Diamand Y., Krylov S., Shmilovich T., Almog R. O., Fishelson N., Sverdlov Y., Torchinsky I., Rosenman G., Inberg A., Berkh O.: Metallization technologies and strategies for plastic based biochips, sensors and actuators for healthcare and medical applications. ECS Transactions, **23**, 243–254 (2009). https://doi.org/10.1149/1.3183726

[13] An D., Lotfian S., Mesbah D., Ayre D., Yoosefinejad A., Thakur V. K., Nezhad H. Y.: Ultra-thin electrospun nanofibers for development of damage-tolerant composite laminates. Materials Today Chemistry, **14**, 100202 (2019). https://doi.org/10.1016/j.mtchem.2019.100202

[14] Mondal K., McMurtrey M. D.: Present status of the functional advanced micro-, nano-printings – A mini review. Materials Today Chemistry, **17**, 100328 (2020). https://doi.org/10.1016/j.mtchem.2020.100328

[15] Bikshapathi M., Mandal S., Mathur G. N., Sharma A., Verma N.: Modification of activated carbon fiber by metal dispersion and surface functionalization for the removal of 2-chloroethanol. Industrial & Engineering Chemistry Research, **50**, 13092–13104 (2011). https://doi.org/10.1021/ie101860e

[16] Lu L., Hu Y., Dai K.: The advance of fiber-shaped lithium ion batteries. Materials Chemistry Today, **5**, 24–33 (2017). https://doi.org/10.1016/j.mtchem.2017.05.003

[17] Bageshlooyafshar B., Vakilian S., Kehtari M., Eslami-Arshaghi T., Rafeie F., Ramezanifard R., Rahchamani R., Mohammadi-Sangcheshmeh A., Mostafaloo Y., Seyedjafari E.: Zinc silicate mineral-coated scaffold improved *in vitro* osteogenic differentiation of equine adipose-derived mesenchymal stem cells. Research in Veterinary Science, **124**, 444–451 (2019). https://doi.org/10.1016/j.rvsc.2017.09.015

[18] Rahaman M. S. A., Ismail A. F., Mustafa A.: A review of heat treatment on polyacrylonitrile fiber. Polymer Degradation and Stability, **92**, 1421–1432 (2007). https://doi.org/10.1016/j.polymdegradstab.2007.03.023

[19] Nataraj S. K., Yang K. S., Aminabhavi T. M.: Polyacrylonitrile-based nanofibers – A state-of-the-art review. Progress in. Polymer Science, **37**, 487–513 (2012). https://doi.org/10.1016/j.progpolymsci.2011.07.001

[20] Katepalli H., Bikshapathi M., Sharma C. S., Verma N., Sharma A.: Synthesis of hierarchical fabrics by electrospinning of PAN nanofibers on activated carbon microfibers for environmental remediation applications. Chemical Engineering Journal, **171**, 1194–1200 (2011). https://doi.org/10.1016/j.cej.2011.05.025

[21] Lee H., Watanabe K., Kim M., Gopiraman M., Song K-H., Lee J. S., Kim I. S.: Handspinning enabled highly concentrated carbon nanotubes with controlled orientation in nanofibers. Scientific Reports, **6**, 37590 (2016). https://doi.org/10.1038/srep37590

[22] Shilpa, Sharma A.: Enhanced electrochemical performance of electrospun Ag/hollow glassy carbon nanofibers as free-standing Li-ion battery anode. Electrochimica Acta, **176**, 1266–1271 (2015). https://doi.org/10.1016/j.electacta.2015.07.093

[23] Karimi-Maleh H., Cellat K., Arıkan K., Savk A., Karimi F., Şen F.: Palladium–nickel nanoparticles decorated on functionalized-MWCNT for high precision non-enzymatic glucose sensing. Materials Chemistry and Physics, **250**, 123042 (2020). https://doi.org/10.1016/j.matchemphys.2020.123042

[24] Grassie N., Hay J. N.: Thermal coloration and insolubilization in polyacrylonitrile. Journal of Polymer Science, **56**, 189–202 (1962). https://doi.org/10.1002/pol.1962.1205616316

[25] Morgan P.: Carbon fibers and their composites. CRC Press, New York (2005).

[26] Bashir Z.: A critical review of the stabilisation of polyacrylonitrile. Carbon, **29**, 1081–1090 (1991). https://doi.org/10.1016/0008-6223(91)90024-D

[27] Zhao W., Lu Y., Wang J., Chen Q., Zhou L., Jiang J., Chen L.: Improving crosslinking of stabilized polyacrylonitrile fibers and mechanical properties of carbon fibers by irradiating with γ-ray. Polymer Degradation and Stability, **133**, 16–26 (2016). https://doi.org/10.1016/j.polymdegradstab.2016.07.018

[28] Houtz R. C.: Orlon acrylic fiber: Chemistry and properties. Textile Research Journal, **20**, 786–801 (1950). https://doi.org/10.1177/004051755002001107

[29] Whitford J., Shinde M., Hunt B., Miller S., Kostogorova-Beller Y.: Perceived color of undoped electrospun polyacrylonitrile nanofibers. Journal of Polymer Science Part B: Polymer Physics, **55**, 1278–1285 (2017). https://doi.org/10.1002/polb.24386

[30] Friedlander H. N., Peebles L. H., Brandrup J., Kirby J. R.: On the chromophore of polyacrylonitrile. VI. Mechanism of color formation in polyacrylonitrile. Macromolecules, **1**, 79–86 (1968). https://doi.org/10.1021/ma60001a014

[31] Park S., Yoo S. H., Kang H. R., Jo S. M., Joh H-I., Lee S.: Comprehensive stabilization mechanism of electron-beam irradiated polyacrylonitrile fibers to shorten the conventional thermal treatment. Scientific Reports, **6**, 27330 (2016). https://doi.org/10.1038/srep27330

[32] Zhang H., Quan L., Xu L.: Effects of amino-functionalized carbon nanotubes on the crystal structure and thermal properties of polyacrylonitrile homopolymer microspheres. Polymers, **9**, 332 (2017). https://doi.org/10.3390/polym9080332

[33] Qiao M., Kong H., Ding X., Hu Z., Zhang L., Cao Y., Yu M.: Study on the changes of structures and properties of PAN fibers during the cyclic reaction in supercritical carbon dioxide. Polymers, **11**, 402 (2019). https://doi.org/10.3390/polym11030402

[34] Gries K., Vieker H., Gölzhäuser A., Agarwal S., Greiner A.: Preparation of continuous gold nanowires by electrospinning of high-concentration aqueous dispersions of gold nanoparticles. Small, **8**, 1436–1441 (2012). https://doi.org/10.1002/smll.201102308

[35] Kara G. K., Moshari M., Rabbani M., Rahimi R.: A novel and green heterogeneous photocatalytic system ($Ca_{0.01}Fe_{2.99}O_4/CaTiO_3$ nanocomposite): Protocol synthesis, characterization, and study of photo-decoloration activity. Materials Chemistry and Physics, **259**, 124062 (2021). https://doi.org/10.1016/j.matchemphys.2020.124062

[36] Boita J., Nicolao L., Alves M. C., Morais J.: Observing Pt nanoparticle formation at the atomic level during polyol synthesis. Physical Chemistry Chemical Physics, **16**, 17640–17647 (2014). https://doi.org/10.1039/c4cp01925c

[37] Aboagye A., Elbohy H., Kelkar A. D., Qiao Q., Zai J., Qian X., Zhang L.: Electrospun carbon nanofibers with surface-attached platinum nanoparticles as cost-effective and efficient counter electrode for dye-sensitized solar cells. Nano Energy, **11**, 550–556 (2015). https://doi.org/10.1016/j.nanoen.2014.10.033

[38] de Azevedo Gonçalves Mota R. C., da Silva E. O., de Menezes L. R.: Effect of the addiction of metal oxide nanoparticles on the physical, chemical and thermal properties of PVA based nanocomposites. Materials Sciences and Applications, **9**, 473–488 (2018). https://doi.org/10.4236/msa.2018.95033

[39] Shi Q., Vitchuli N., Nowak J., Caldwell J. M., Breidt F., Bourham M., Zhang X., McCord M.: Durable antibacterial Ag/polyacrylonitrile (Ag/PAN) hybrid nanofibers prepared by atmospheric plasma treatment and electrospinning. European Polymer Journal, **47**, 1402–140 (2011). https://doi.org/10.1016/j.eurpolymj.2011.04.002

[40] Múgica-Vidal R., Sainz-García E., Álvarez-Ordóñez A., Prieto M., González-Raurich M., López M., López M., Rojo-Bezares B., Sáenz Y., Alba-Elías F.: Production of antibacterial coatings through atmospheric pressure plasma: A promising alternative for combatting biofilms in the food industry. Food and Bioprocess Technology, **12**, 1251–1263 (2019). https://doi.org/10.1007/s11947-019-02293-z

[41] Karacan I., Erdogan G.: The influence of thermal stabilization stage on the molecular structure of polyacrylonitrile fibers prior to the carbonization stage. Fibers and Polymers, **13**, 295–302 (2012). https://doi.org/10.1007/s12221-012-0295-5

[42] Arbab S., Zeinolebadi A.: A procedure for precise determination of thermal stabilization reactions in carbon fiber precursors. Polymer Degradation and Stability, **98**, 2537–2545 (2013). https://doi.org/10.1016/j.polymdegradstab.2013.09.014

[43] Karbownik I., Fiedot M., Rac O., Suchorska-Woźniak P., Rybicki T., Teterycz H.: Effect of doping polyacrylonitrile fibers on their structural and mechanical properties. Polymer, **75**, 97–08 (2015). https://doi.org/10.1016/j.polymer.2015.08.015

[44] Dang W., Liu J., Wang X., Yan K., Zhang A., Yang J., Chen L., Liang J.: Structural transformation of polyacrylonitrile (PAN) fibers during rapid thermal pretreatment in nitrogen atmosphere. Polymers, **12**, 63 (2020). https://doi.org/10.3390/polym12010063

[45] Ghorpade R. V., Cho D. W., Hong S. C.: Effect of controlled tacticity of polyacrylonitrile (*co*)polymers on their thermal oxidative stabilization behaviors and the properties of resulting carbon films. Carbon, **121**, 502–511 (2017). https://doi.org/10.1016/j.carbon.2017.06.015

[46] Coleman M. M., Petcavich R. J.: Fourier transform infrared studies on the thermal degradation of polyacrylonitrile. Journal of Polymer Science Part B: Polymer Physics, **16**, 821–832 (1978). https://doi.org/10.1002/pol.1978.180160507

[47] Frank E., Hermanutz F., Buchmeiser M. R.: Carbon fibers: Precursors, manufacturing, and properties. Macromolecular Materials and Engineering, **297**, 493–501 (2012). https://doi.org/10.1002/mame.201100406

[48] Arbab S., Zeinolebadi A.: Quantitative analysis of the effects of comonomers and heating conditions on the stabilization reactions of polyacrylonitrile fibers as carbon fiber precursors. Polymer Degradation and Stability, **139**, 107–116 (2017). https://doi.org/10.1016/j.polymdegradstab.2017.04.003

[49] Fitzer E., Müller D. J.: The influence of oxygen on the chemical reactions during stabilization of pan as carbon fiber precursor. Carbon, **13**, 63–69 (1975). https://doi.org/10.1016/0008-6223(75)90259-6

[50] Elagib T. H., Hassan E. A., Liu B., Han K., Yu M.: Evaluation of composite PAN fibers incorporated with carbon nanotubes and titania and their performance during the microwave-induced pre-oxidation. Carbon Letters, **30**, 235–245 (2020). https://doi.org/10.1007/s42823-019-00092-2

[51] Wang Y., Yang Q., Shan G., Wang C., Du J., Wang S., Li Y., Chen X., Jing X., Wei Y.: Preparation of silver nanoparticles dispersed in polyacrylonitrile nanofiber film spun by electrospinning. Materials Letters, **59**, 3046–3049 (2005). https://doi.org/10.1016/j.matlet.2005.05.016

[52] Ye X., Sha J., Jiao Z., Zhang L.: Size effect on structure and infrared behavior in nanocrystalline magnesium oxide. Nanostructured Materials, **8**, 945–951 (1997). https://doi.org/10.1016/S0965-9773(98)00011-7

[53] Matsumura Y., Enomoto Y., Sugiyama M., Akamatsu K., Nawafune H.: Direct metallization of nickel on polymeric template patterns for fabrication of copper circuits on glass substrates. Journal of Materials Chemistry A, **18**, 5078–5082 (2008). https://doi.org/10.1039/B808267G

[54] Ahmadi T., Monshi A., Mortazavi V., Fathi M. H., Sharifi S., Kharaziha M., Khazdooz L., Zarei A., Dehaghani M. T.: Fabrication and characterization of polycaprolactone fumarate/gelatin-based nanocomposite incorporated with silicon and magnesium *co*-doped fluorapatite nanoparticles using electrospinning method. Materials Science and Engineering: C, **106**, 110172 (2020). https://doi.org/10.1016/j.msec.2019.110172

[55] Wang D., Yue Y., Wang Q., Cheng W., Han G.: Preparation of cellulose acetate-polyacrylonitrile composite nanofibers by multi-fluid mixing electrospinning method: Morphology, wettability, and mechanical properties. Applied Surface Science, **510**, 145462 (2020). https://doi.org/10.1016/j.apsusc.2020.145462

[56] Ziglio A. C., Sardela M. R., Gonçalves D.: Wettability, surface free energy and cellulose crystallinity for pine wood (*Pinus sp*.) modified with chili pepper extracts as natural preservatives. Cellulose, **25**, 6151–6160 (2018). https://doi.org/10.1007/s10570-018-2007-9

[57] Huan S., Bai L., Liu G., Cheng W., Han G.: Electrospun nanofibrous composites of polystyrene and cellulose nanocrystals: Manufacture and characterization. RSC Advances, **5**, 50756–50766 (2015). https://doi.org/10.1039/C5RA06117B

[58] Wong S-C., Baji A., Leng S.: Effect of fiber diameter on tensile properties of electrospun poly(ε-caprolactone). Polymer, **49**, 4713–4722 (2008). https://doi.org/10.1016/j.polymer.2008.08.022

[59] Tijing L. D., Woo Y. C., Shim W-G., He T., Choi J-S., Kim S-H., Shon H. K.: Superhydrophobic nanofiber membrane containing carbon nanotubes for high-performance direct contact membrane distillation. Journal Membrane Science, **502** 158–170 (2016). https://doi.org/10.1016/j.memsci.2015.12.014

[60] Rahmani H., Najafi S. H. M., Ashori A., Fashapoyeh M. A., Mohseni F. A., Torkaman S.: Preparation of chitosan-based composites with urethane cross linkage and evaluation of their properties for using as wound healing dressing. Carbohydrate Polymers, **230**, 115606 (2020). https://doi.org/10.1016/j.carbpol.2019.115606

[61] Sun L., Guo P., Ke P., Li X., Wang A.: Synergistic effect of Cu/Cr *co*-doping on the wettability and mechanical properties of diamond-like carbon films. Diamond and Related Materials, **68**, 1–9 (2016). https://doi.org/10.1016/j.diamond.2016.05.006

[62] Zisman W. A.: Relation of the equilibrium contact angle to liquid and solid constitution. in 'Contact angle, wettability, and adhesion, advances in chemistry' (ed.: Fowkes F. M.) ACS Publications, Washington, 1–51 (1964). https://doi.org/10.1021/ba-1964-0043.ch001